Therapeutic Potential of Omega-5 Fatty Acids in Ovarian Cancer

Jingjia Mo †, Isabella Mendieta †, Alexander J. Adams, Katherine Wiest, Hannah Lee, Victoria Gorman, Rachel Koo, Santiago Garcia, Ethan Nguyen, Aaron Lee, Jihua Feng, Zhiqing Huang *

Posted Date: 10 February 2026

doi: 10.20944/preprints202602.0821.v1

Keywords: ovarian cancer; punicic acid; ferroptosis; mitochondrial dysfunction; free fatty acids; cisplatin synergy; tumor microenvironment

 doi:10.20944/preprints202602.0821.v1

Article

Therapeutic Potential of Omega-5 Fatty Acids in Ovarian Cancer

Jingjia Mo [1,2,†], Isabella Mendieta [1,†], Alexander J. Adams [1], Katherine Wiest [1], Hannah Lee [1], Victoria Gorman [1], Rachel Koo [1], Santiago Garcia [1], Ethan Nguyen [1], Aaron Lee [1], Jihua Feng [1,3] and Zhiqing Huang [1,*]

[1] Division of Reproductive Sciences, Department of Obstetrics and Gynecology, Duke University School of Medicine, Durham, NC
[2] Department of General Practice, The Second Affiliated Hospital of Guangxi Medical University, Nanning, Guangxi, China
[3] Department of Emergency, The Second Affiliated Hospital of Guangxi Medical University, Nanning, Guangxi, China
* Correspondence: zhiqing.huang@duke.edu; Tel.: 919.684.1396
† Co-first author due to equal contributions.

Highlights

What are the main findings?

- Punicic Acid kills ovarian cancer cells, spares normal cells, and enhances cisplatin efficacy.
- Punicic Acid triggers ferroptosis and alters lipid metabolism, mitochondrial function, and key inflammatory and tumor-related pathways in ovarian cancer cells.

What are the implications of the main findings?

- This study suggests that combining punicic acid with cisplatin may allow lower chemotherapy doses while maintaining or enhancing antitumor efficacy, potentially improving clinical tolerability.
- These findings define the mechanisms underlying punicic acid's selective toxicity, providing insight into ovarian cancer cell vulnerabilities.

Abstract

Ovarian cancer (OC) remains the deadliest gynecological malignancy, with aged tumor microenvironments linked to poorer outcomes. Our prior work identified reduced levels of free fatty acids (FFAs) within tumor-surrounding adipose tissue of aged OC xenograft rats compared to younger counterparts. In this study, we investigated the therapeutic potential of one such FFA, punicic acid (PunA). We evaluated PunA's effects on OC and normal cell viability and compared its activity with that of its structural isomer, α-eleostearic acid (α-ESA). Both compounds decreased OC cell viability; however, α-ESA was cytotoxic to normal cells, whereas PunA selectively impaired OC cell viability while sparing normal cells. Additionally, PunA enhanced cisplatin efficacy, demonstrating its potential for use in combination therapy to reduce cisplatin dosage and toxicity without compromising antitumor activity. Mechanistically, PunA induced ferroptosis in OC cells while sparing normal cells by differently modulating lipid peroxidation, fatty acid oxidation, and mitochondrial function. Transcriptomic profiling further revealed broad gene expression and pathway reprogramming in PunA-treated OC and normal cells. In a preliminary C57BL/6J-ID8 OC mouse model, PunA suppressed tumor growth. Collectively, these findings identify PunA as a promising therapeutic candidate for OC, acting through ferroptosis and mitochondrial dysfunction, and enhancing cisplatin efficacy while sparing normal cells.

Keywords: ovarian cancer; punicic acid; ferroptosis; mitochondrial dysfunction; free fatty acids; cisplatin synergy; tumor microenvironment

 doi:10.20944/preprints202602.0821.v1

1. Introduction

Ovarian cancer (OC) is one of the leading causes of cancer-related deaths in women, with a lifetime risk factor of approximately 1 in 91 [1,2]. In its early stages, OC does not exhibit specific symptoms and is thus mostly diagnosed when it has already reached more advanced stages with aggressive metastasis in the peritoneal cavity and even distant organs [3]. Most OC cases occur in older women, with a median age at diagnosis of 63 years [2]. In addition, cancer recurrence and metastasis, which are among the most common complications for OC, often increase with age [4]. The combination of many factors, such as aging, lack of effective diagnostic strategies, late detection, development of resistance to therapy, and frequent recurrence, leads to a relatively high mortality rate in OC patients [3]. Continued research is urgently needed to identify therapeutic strategies that not only target the aggressive and resistant nature of OC but also address age-related changes in tumor biology to improve early detection and treatment outcomes.

Aging significantly impacts OC progression and metastasis, primarily through alterations in both the systemic macroenvironment and the tumor microenvironment (TME) [5,6]. The TME consists of both non-cellular elements, such as the extracellular matrix (ECM), and cellular components—including immune cells, fibroblasts, endothelial cells, and adipocytes—all of which create a more permissive environment for cancer cell survival, growth, and spread [6]. Adipose tissue (AT), also referred to as the adipose tumor microenvironment (AME), represents a major component of the TME in OC and plays a significant role in promoting both cancer initiation and disease progression [7,8]. OC begins its progression in the peritoneal cavity, subsequently spreading to the AT within the intraperitoneal cavity, specifically in the omentum [9]. The interaction between the OC cells and the AT in the omentum induces morphological changes in adipocytes, leading to the formation of cancer-associated adipocytes (CAAs) [10]. These adipocytes contribute to the progression of OC through multiple mechanisms, including tumor growth, chemoresistance, metastasis, and even recurrence [11]. The impact of adipocytes on OC is thus an important direction of research, especially because AT is one of the earliest organs to change in response to aging [12]. It was largely unknown, however, the extent to which these age-related changes impact OC cells, OC progression, and chemotherapies.

To address this gap, we investigated the roles of aging on the adipocyte-rich TME in an OC xenograft rat model through lipidomic and transcriptomic profiling of tumor-surrounding AT [13]. In this previous study, our findings demonstrated that aged RNU nude rats (12 months old) were more susceptible to and exhibited more aggressive tumor development, with 100% (13 out of 13 rats) of the aged rats forming tumors, compared to 68.75% (11 out of 16 rats) of the young rats (6 weeks old). Median tumor volumes of 17.6 cm^3 and 1.1 cm^3 were observed in the aged and younger cohorts, respectively. Using tumor-surrounding AT tissues from aged OC rats, RNA sequencing analysis revealed notable upregulation of genes associated with inflammation and lipid regulation, including *S100a8*, *S100a9*, *Lcn2*, *C3*, and *Pnpla3*, when compared to the AT from young OC rats. In addition, aged OC ATs exhibited significantly higher ($p < 0.05$) infiltration of neutrophils, dendritic cells, and CD4+ T-cells (non-regulatory) compared to their ATs before tumor formation, reflecting pro-inflammatory shifts that are conducive to cancer progression. These immune alterations were strongly correlated with changes in *S100a8*/*a9* expression and lipid levels.

Lipidomic profiling further revealed a significant downregulation ($p < 0.05$) of multiple free fatty acid (FFA) species in tumor-surrounding AT from aged OC rats compared to AT from their younger counterparts [13]. Among these, an FFA 18:3 (omega-5), chemically designated (9E,11Z,13E)-octadecatrienoic acid and more commonly known as punicic acid (PunA), showed the most pronounced decrease [13]. Interestingly, preliminary in vitro studies demonstrated that PunA diverged from other lipid alterations by exhibiting antitumor properties, as it significantly inhibited viability across three OC cell lines: A2780, HEYA8, and CAOV2 ($p < 0.001$) [13].

Building on this finding, the current study investigates the chemotherapeutic potential of FFAs in OC with a focus on PunA. We also examined another FFA 18:3 omega-5 member, alpha-eleostearic

 doi:10.20944/preprints202602.0821.v1

acid (α-ESA), because these two conjugated trienoic fatty acids share nearly identical molecular structures, differing only in the geometric arrangement of the double bond at the omega-5 position. PunA contains Δ9 cis, Δ11 trans, and Δ13 cis double bonds, while α-ESA possesses Δ9 cis, Δ11 trans, and Δ13 trans double bonds. As essential nutrients, neither compound can be synthesized endogenously and must be obtained through the diet [14]. PunA is derived primarily from pomegranate (*Punica granatum*) seed oil, while α-ESA is found predominantly in tung (*Aleurites fordii*) and bitter ground (*Momordica charantia*) seed oils [15]. Both compounds have garnered considerable attention due to their reported health benefits.

PunA, in particular, is known for its antidiabetic, anti-obesity, anti-inflammatory, and anticancer properties14. Nugteren *et al.* demonstrated that PunA inhibits cyclooxygenase activity, thereby reducing prostaglandin synthesis and contributing to its anti-inflammatory effects [16]. Using *in vitro* cancer models, PunA has been shown to reduce the viability of LNCaP (prostate cancer) cells at concentrations above 10 μM through pro-apoptotic and growth-inhibitory pathways [17]. In MDA-MB-231 and MDA-ERα7 (breast cancer) cell lines, a 40 μM dose of PunA reduced cell growth by over 90% and triggered apoptosis in more than 85% of the cells [18]. Notably, Quitmeyer *et al.* reported that MCF-10 (non-tumorigenic breast epithelial) cells were more sensitive to PunA-induced cytotoxicity than breast cancer MCF-7 cells at low concentrations [19].

The anticancer activity of α-ESA has also been demonstrated across a range of human cancer cell lines, where it exhibits dose-dependent cytotoxic effects in DLD-1 (colorectal cancer), HepG2 (liver cancer), and A549 (lung cancer) cells [20]. In breast cancer MCF-7 cells, Zhang *et al.* have demonstrated that α-ESA upregulates several pro-apoptotic markers, including PPAR-γ, p21, Bax, p53, and caspase-3 [21].

In the context of OC, natural compounds related to PunA and α-ESA have demonstrated anticancer effects. For example, pomegranate fruit juice and two of its principal constituents, ellagic acid and luteolin, suppress OC proliferation, migration, and progression by downregulating expression of MMP-2 and MMP-9 in A2780 cells (ovarian cancer) and nude mouse models [22]. Similarly, bitter melon and its bioactive compounds, such as kuguacin J, inhibit OC by inducing apoptosis, suppressing proliferation and migration, altering cancer cell metabolism, and enhancing the efficacy of chemotherapy drugs, all with minimal toxicity in preclinical models [23,24]. These effects are mediated, at least in part, through the activation of AMPK signaling and the inhibition of oncogenic pathways, including mTOR, AKT/ERK, and FOXM1 [25]. Despite the promising findings for related compounds, no studies have evaluated the anticancer potential of PunA and α-ESA in OC, including their cytotoxic effects on tumor-surrounding normal cells or the underlying mechanisms involved. Evidence from their efficacy in other cancers underscores the need to address this gap to determine whether PunA and α-ESA share, or even surpass, the therapeutic properties of their structurally related counterparts.

We previously demonstrated that FFAs are downregulated in aged OC xenografts and that certain FFA compounds may possess anticancer activity [13]. In the present study, we investigated the therapeutic potential of two structurally related FFAs, PunA and α-ESA, in treating OC, a disease highly prevalent in aged women and recognized as an age-associated cancer. Given their close structural similarity and prior evidence of anticancer properties, we directly compared the effects of PunA and α-ESA. To assess cell-specificity and potential cytotoxicity, we tested normal ovarian epithelial cells, normal fallopian tube (NFT) cells, and adipocytes commonly found in the tumor-surrounding AT. Because chemoresistance is a major challenge in OC, we also studied the effects of PunA on chemo-resistant OC cells. In addition, we investigated how fats, as a major component of OC tissues, influence PunA's chemotherapeutic effects. To better understand the differential functions of PunA in cancer and normal cells, we conducted an in-depth study of mechanisms involving peroxisome proliferator-activated receptor gamma (PPARγ), ferroptosis, lipid peroxidation, and mitochondrial function. We further explored gene expression profiling and molecular pathways through which PunA may exert its effects. A clearer understanding of PunA's functions will clarify how, in the context of OC, it preferentially targets cancer cells while sparing

 doi:10.20944/preprints202602.0821.v1

normal cells. This knowledge is crucial for opening new avenues in the development of effective, low-toxicity chemotherapeutic treatments for OC patients.

2. Materials and Methods

2.1. Cell Lines and Reagents

The OC cell lines, including HEYA8, CAOV2, A2780, 41M, 41M-cisR (cisplatin resistant cell line generated from 41M), A2780, A2780-cisR (cisplatin resistant cell line generated from A2780), and mouse preadipocyte 3T3-L1 cells line were initially purchased from ATCC and maintained in Duke University Ovarian Cancer Cell Line Bank. OC cells were maintained in RPMI 1640 (Thermo Fisher, Cat # A4192301) with 10% FBS (Thermo Fisher, Cat# A5256801) and 1% Penicillin-Streptomycin (P/S, MilliporeSigma, Cat #p4333). The mouse preadipocyte 3T3-L1 cells were maintained in DMEM medium with high glucose (MilliporeSigma, Cat # D5796), 10% Bovine Calf Serum (BCS, MilliporeSigma, Cat # 12133C) and 1% P/S. The mouse ID8-luciferase-expressing ovarian carcinoma cells (ID8-Luc) were generously provided by Dr. Ashley Chi at Duke University, and the cells were cultured in DMEM medium with high glucose (MilliporeSigma, Cat # D5796), 10% Bovine Calf Serum (BCS, MilliporeSigma, Cat # 12133C) and 1% P/S. ID8-Luc cells are genetically engineered mouse ovarian cancer cells that stably express the firefly luciferase protein. When the substrate luciferin is added, the luciferase enzyme catalyzes a reaction that produces bioluminescence, enabling the detection of cancer cells using the IVIS imaging system in live animals. The normal ovarian scraped epithelial cells E7 has obtained as gift from the Japanese Collection of Research Bioresources (JCRB) Cell Bank. The NFT scraped epithelial cells P201 and P211 were initially obtained from a patient without malignant disease. E7 and P201 cells were maintained in RPMI 1640 (ThermoFisher, Cat # A4192301) with 10% FBS (Thermo Fisher, Cat# A5256801) and 1% Penicillin-Streptomycin (P/S, MilliporeSigma, Cat # p4333). All the cell lines were incubated at 37°C in a humidified chamber with 5% CO_2. All cell lines were genetically authenticated prior to use by the Duke University DNA Analysis Facility to verify their identity, purity, and authenticity. Additionally, all cell lines were tested and confirmed to be free of mycoplasma contamination by the Duke Cell Culture Facility. Punicic acid (PunA; 9Z,11E,13Z-octadecatrienoic acid; Cat # 26057) and α-eleostearic acid (α-ESA; 9Z,11E,13E-octadecatrienoic acid; Cat # 10008349) were purchased from Cayman Chemical (Ann Arbor, MI, USA). Cisplatin (cis-diamminedichloroplatinum (II); Cat # HY-17394) and Ferrostatin-1 (Fer-1, Cat # HY-100579) were purchased from MedChemExpress (Monmouth Junction, NJ, USA).

2.2. Cell Treatments

2.2.1. PunA, α-ESA, and Cisplatin Treatment of OC and Normal Cell Lines

The OC cell line HEYA8 (2,000 cells/well) and normal cell lines NFT P201 (2,000 cells/well), NFT P211 (2,000 cells/well), ovarian epithelial E7 (4000 cells/well), and mouse preadipocyte 3T3-L1 (5,000 cells/well) were seeded into 96-well plates after reaching ~70% confluency in RPMI medium supplemented with 10% FBS and penicillin/streptomycin (P/S). Cell viability and counts were determined prior to seeding using a hemocytometer and Trypan Blue staining (Thermo Fisher, Cat. # 15250061). After 24 h incubation at 37 °C with 5% CO_2, cells were treated with vehicle control (methanol; VWR, Cat. # BDH1135-4LP), varying concentrations of PunA or α-ESA, or 20 μM cisplatin. Each treatment condition was performed in sextuplicate. Research manuscripts reporting large datasets that are deposited in a publicly available database should specify where the data have been deposited and provide the relevant accession numbers. If the accession numbers have not yet been obtained at the time of submission, please state that they will be provided during review. They must be provided prior to publication.

2.2.2. Combinational Chemo-Treatment

The OC cell line HEYA8 (2000 cells/well) was treated with cisplatin alone or in combination with PunA. Treatment groups consisted of vehicle control (methanol), 20 μM PunA, 20 μM cisplatin, and

 doi:10.20944/preprints202602.0821.v1

20 μM PunA + 20 μM cisplatin. The treatment was performed for 48 h, followed by an MTS assay to assess cell viability relative to control. Each treatment condition was performed in sextuplicate.

2.2.3. PunA Treatment on Cisplatin Resistant Cell Lines

The experiment was performed separately with two parental OC cell lines, 41M and A2780, and their cisplatin resistant pairs, 41M-cisR and A2780-cisR. Each cell line was cultured in RPMI medium supplemented with 10% FBS and 1% P/S until reaching approximately 80% confluency, then seeded into 96-well plates, at 8000 cells/well for M41 and 41M-cisR, and 3000 cells/well for A2780 and A2780-cisR. After 24 hours of incubation, the cells were treated with PunA at concentrations ranging from 0 μM to 120 μM for 48 h at 37°C with 5% CO_2. An MTS assay (as described below) was performed to determine cell viability and to compare between the parental and cisR cell pairs using the method indicated in the statistical analysis. Each treatment condition was performed in sextuplicate. The OC cell line HEYA8 (2000 cells/well) was treated with cisplatin alone or in combination with PunA. Treatment groups consisted of vehicle control (methanol), 20 μM PunA, 20 μM cisplatin, and 20 μM PunA + 20 μM cisplatin. The treatment was performed for 48 h, followed by an MTS assay to assess cell viability relative to control. Each treatment condition was performed in sextuplicate.

2.2.4. PunA Treatment on OC Cells in High Versus Low Fat Medium

The high-fat conditioned medium was generated from differentiated 3T3-L1 preadipocytes following an established protocol from Abcam (Cat # ab287843). This protocol uses a "differentiation cocktail" containing insulin, dexamethasone, and 3-isobutyl-1-methylxanthine (IBMX), followed by a maintenance medium with a lower concentration of these components. The medium from the undifferentiated 3T3-L1 was used as low-fat condition control. HEYA8 cells were maintained in RPMI medium supplemented with 10% FBS and 1% penicillin-streptomycin (P/S) until reaching approximately 80% confluency, then seeded at 3000 cells per well into 96-well plates and incubated for 24 h at 37°C with 5% CO_2. HEYA8 cells were then treated with PunA at concentrations ranging from 0 to 100 μM in either differentiated or undifferentiated medium conditions and incubated for 48 h. Cell viability was measured by MTS assay to evaluate resistance to PunA in high fat versus control media. Each treatment condition was performed in sextuplicate.

2.2.5. Ferrostatin-1 Treatment

The OC cell lines HEYA8 and A2780 were cultured to approximately 70% confluency and seeded into 96-well plates at 2000 cells/well for HEYA8 and 3000 cells/well for A2780. After 24 h of incubation at 37°C with 5% CO_2, cells were treated with vehicle control (methanal, MtOH), 2 μM of Fer-1, PunA, and Fer-1+PunA. PunA was used at 25 μM for HEYA8 cells and 30 μM PunA for A2780 cells. Cells were treated for 48 h prior to assessment of viability using the MTS assay (see below for the protocol). Each treatment condition was performed in sextuplicate.

2.3. Cell Viability Assay (MTS Assay)

The CellTiter 96® AQueous One Solution Cell Proliferation Assay was performed with 3-(4,5-dimethylthiazol-2-yl)-5-(3-carboxymethyl phenyl)-2-(4-sulfophenyl)-2H-tetrazolium (Promega, Cat # G3582), a colorimetric method (MTS Assay) for determining cell viability. After the specified incubation period for each test, 20 μL of the MTS solution was added to each well of the 96-well microplates, each containing 100 μL of a mixture of cells and treatment medium. Following a 1–4 h incubation at 37°C, the absorbance for cell viability was measured at 490 nm using the FluoStar Omega Plate Reader.

2.4. Lipid Peroxidation Assay by Flow Cytometry

The OC cell line HEYA8 and the NFT epithelial cell line P201 were used for this test. HEYA8 and P201 cells at 3×10^5 were seeded into each well of 6-well plates and incubated in RPMI 1640 medium

 doi:10.20944/preprints202602.0821.v1

with 10% FBS and 1% P/S at 37°C and 5% CO_2 for 24 h. Following incubation, the cells were divided into three treatment groups: untreated control, vehicle control (same volume of methanol as for PunA), and 10 μM PunA treatment. All groups were incubated for 48 h before BODIPY™ 581/591 C11 (Thermo Fisher Scientific, Cat# D3861) assay. This treatment duration was specifically chosen to allow enough time for PunA to be incorporated into cellular membranes and have its hypothesized effects on lipid metabolism and oxidation. After 48 h of treatment, the HEYA8 and P201 cells were incubated in 10 μM concentration of BODIPY™ 581/591 C11 undecanoic acid (Lipid Peroxidation Sensor) within the medium for 30 min at 37°C. This sensor probe undergoes a shift upon oxidation, which allows for the detection and quantification of lipid peroxidation in live cells. After incubation, the media was removed, and the cells were washed with Dulbecco's Phosphate Buffered Saline (PBS). The cells were collected using Trypsin in 15-mL tubes and washed with PBS three times, centrifuging for 5 min at 2000 RPM after each wash. After the third wash, 1 mL of PBS was added to resuspend the cells, and the cells were filtered through the mesh attached to the flow cytometry tubes to ensure single-cell suspension. The cells were imaged using the FortessaX20 machine within 2 h of staining to maintain signal integrity, and the fluorescence was read at two separate wavelengths: one at excitation/emission of 581/591 nm (Texas Red® filter set) to detect the reduced dye, and the other at excitation/emission of 488/510 nm (traditional FITC filter set) to detect the oxidized dye. This test was repeated twice for both cell lines to quantitatively assess the shift from Texas Red to Green FITC which indicates lipid peroxidation in response to different treatment conditions. The two tests were analyzed using Student's t-test to compare lipid peroxidation levels under PunA treatment versus vehicle control.

2.5. Fatty Acid Oxidation (FAO) Assay

Four cell lines including two OC cell lines, A2780 and HEYA8, and two noncancerous cell lines, E7 and P201, were cultured in RPMI 1640 Medium with 10% FBS and 1% P/S at 37°C and 5% CO_2. Once the cells reached 80% confluence, they were split into 10 cm petri dishes (P10) for treatment, with approximately 1×10^6 cells per dish per cell line. The cells were then treated with PunA or with the vehicle control, methanol, at the same volume as PunA. For the HEYA8 cell line, a 10 μM treatment of PunA was used. For the A2780, E7, and P201 cell lines, 25 μM treatments of PunA were used. Treatment concentrations were chosen based on our studies on cell viability using varying PunA doses. The treatment was administered 6 h after cell seeding. 48 h post-treatment, the adherent cells were dissociated using trypsin and neutralized with RPMI + 10% FBS growth medium. Cells were collected and pelleted at 3000 rpm for 5 min in a 4°C centrifuge. The following steps were then performed with the Fatty Acid Oxidation Kit (Abcam, Cat # ab118183) according to the procedure from the manufacturer. Briefly, the cells were resuspended in PBS to a concentration of $2–5 \times 10^6$ cells/mL. Fixation was performed using 4% paraformaldehyde at room temperature for 15 minutes. Fixed cells were then incubated in a 1× Permeabilization Buffer (0.1% Triton X-100 in PBS) for 15 min at room temperature. The cells were then blocked in 1x Incubation Buffer (10% Blocking Buffer with 0.1% Triton X-100 in PBS) for 15 min at room temperature. Then, cells were incubated with primary antibodies against the mitochondrial trifunctional protein subunit alpha (HADHA) at 1:50, or the IgG isotype control prepared in the 1x Incubation Buffer for 24 h at 4°C. After washing, with a 1x Wash Buffer (0.05% Tween-20, 1% Blocking Buffer in PBS) the cells were incubated for 1 h in the dark at room temperature with a fluorochrome-conjugated goat anti-mouse secondary antibody (Alexa Fluor® 488) at 1:100 dilution in the 1x Incubation Buffer. After final washes, cells were resuspended in PBS at 1×10^6 cells/mL and transferred from Eppendorf tubes through a cell strainer and into 25 mL polystyrene tubes for flow cytometry analysis. Using the BD FACSCanto-II machine, fluorescence signals were collected for each sample and subsequently analyzed. To assess FAO activity across different cell lines, the percentage of cells expressing the HADHA protein was measured. Fluorescent intensity in the P2 and P3 gates, which are gated from the parent population, P1, were utilized as indicators of HADHA presence. The P1 gate identifies the total viable cell population, while the P2

 doi:10.20944/preprints202602.0821.v1

and P3 gates identify the cell populations that express the HADHA protein. Comparisons were made between IgG controls and HADHA-stained samples in both untreated and PunA-treated groups. The difference in HADHA-positive cells between the treated and untreated conditions was used to calculate the FAO difference, representing relative changes in FAO activity.

2.6. Measurement of Oxygen Consumption Rate (OCR)

The OC cells HEYA8 and normal fallopian tube cells P201 were seeded into Seahorse XF cell culture microplates (Agilent, Cat # 103793-100) at a density of 15×10^3 cells/well and 20×10^3 cells/well, respectively, and incubated overnight. Cells were then treated with either vehicle control (methanol, MeOH) or PunA at concentrations of 20 μM, 40 μM, and 60 μM for 48 h. Then, the oxygen consumption rate (OCR) was measured using the XFe96 Extracellular Flux Analyzer (Seahorse Bioscience) at Duke Core Facility. One hour prior to measurement, the culture medium was replaced with Seahorse assay medium (Agilent, Cat # 103680-100) supplemented with 10 mM glucose, 2 mM glutamine, and 1 mM sodium pyruvate (Agilent, Cat # 103680-100). The following compounds were sequentially injected during the assay: 1.5 μM oligomycin, 1.5 μM FCCP, and 0.75 μM rotenone + 0.75 μM antimycin A (Agilent, Cat # 103010-100). OCR was measured according to the XF Cell Mito Stress Test protocol from the manufacturer. The OCR measurements were normalized with the protein concentrations in each well of the cell culture plate which were determined using the Pierce™ BCA Protein Assay Kit (Cat # 23225; Thermo Fisher Scientific), following the manufacturer's instructions.

2.8. Peroxisome Proliferator-Activated Receptor Gamma (PPAR-γ) Assay

HEYA8 and P201 cells were seeded in 10-centermiter petri-dishes at densities of 4×10^5 cells/plate and 1×10^6 cells/plate, respectively. After overnight incubation, cells were treated with either vehicle control (methanal, MeOH) or various concentrations of PunA for 48 hours. Following treatment, cells were scraped, and total cellular proteins were extracted for analysis. PPAR-γ protein levels were quantified using Human PPAR-gamma ELISA kit (MyBioSource, Cat # MBS2503174) according to the manufacturer's instructions. Protein concentrations were normalized to total protein content determined using BCA assay. The PPAR-γ assay was performed in triplicate.

2.9. Tumor Development in C57BL/6J Mouse Model

An OC model was established in 10 female C57BL/6J mice, including five 8-week-old mice (young) purchased from Charles River and five 19-month-old mice (aged) obtained from the National Institute on Aging (NIA, USA). All mice were maintained under Specific Pathogen-Free (SPF) conditions. Each mouse received a single intraperitoneal (IP) injection of 5×10^6 ID8-Luc ovarian carcinoma cells suspended in 200 μL of a 1:1 mixture of Matrigel and PBS. Tumor formation and growth were monitored by IVIS bioluminescence imaging on days 11, 18, and 40 after ID8 cell injection. On day 40, all mice were euthanized under IACUC-approved protocols using CO_2 asphyxiation as the primary method followed by bilateral thoracotomy as the secondary method.

2.10. PunA Preventive Treatment Using C57BL/6J Mouse Model

Four female C57BL/6J mice (8 weeks old) were purchased from Charles River and maintained under Specific Pathogen-Free (SPF) conditions. All mice received a single intraperitoneal (IP) injection of 5×10^6 ID8-luc ovarian carcinoma cells suspended in 200 μL of a 1:1 mixture of Matrigel and PBS. Three days later, the mice were randomly assigned to control and treatment groups. One mouse was used as a vehicle control, and the remaining three mice were treated with PunA. PunA was dissolved in 50% methanol and administered via IP injection at a dose of 30 μg in 100 μL per mouse once daily, starting 3 days after tumor cell injection, and continued for 3 weeks. Control mice received the vehicle only (100 μL of 50% methanol). After 3 weeks, all mice were euthanized under IACUC-approved protocols, using CO_2 asphyxiation as the primary method followed by bilateral

 doi:10.20944/preprints202602.0821.v1

thoracotomy as the secondary method. Tumor formation and growth were monitored weekly by IVIS bioluminescence imaging.

2.11. IVIS Bioluminescence Imaging

Bioluminescence imaging was performed using the IVIS Spectrum (PerkinElmer, Waltham, MA) at Duke IVIS imaging core. Mice were anesthetized and maintained with 2% isoflurane during the imaging. D-luciferin potassium salt was administered via intraperitoneal (IP) injection at a dose of 150 mg/kg per mouse. Imaging was conducted 10–15 min post-injection. Image acquisition and quantitative analysis of total photon flux (photons/sec) were performed with Living Image software (PerkinElmer, version 4.3.1). Regions of interest were defined for each animal, and total flux measurements were calculated with background correction.

2.12. RNA Extraction and RT-qPCR

Total RNA was extracted using RNA STAT60 Reagent® (Cat # CS-111, Tel-Test). The RNA concentration was determined using Nano-drop2000. RT-qPCR was carried out using 300 ng of RNA per reaction from the MtOH control and PunA-treated HEYA8 cells in a 20 µL reaction volume using the SuperScript IV One-Step RT-PCR kit (Cat # 12594025, Thermo Fisher) according to the protocol provided by the manufacturer with Taqman probes for the genes of Solute Carrier Family 7 Member 11 (SLC7A11) and Glutathione-specific gamma-glutamylcyclotransferase 1 (CHAC1). A probe for the GAPDH gene was used in every RT-qPCR reaction as an internal control for each gene expression analysis.

2.13. RNA Extraction and RNA Sequencing

OC cell lines (HEYA8, A2780) and normal epithelial cells (P201, E7) were treated with PunA (15 µM for HEYA8 and A2780; 20 µM for P201 and E7) or vehicle control (16.7 µL methanol in 10 mL medium) for 48 h. Total RNA was extracted using RNA STAT60 Reagent® (Cat # CS-111, Tel-Test), and sequencing was performed by Admera Health (South Plainfield, NJ, USA). Differential expression analysis was performed for three comparisons:

1. CellLine_Cancer_vs_Normal, comparing ovarian cancer cell lines (HEYA8 and A2780) with normal fallopian tube epithelial cell lines (P201 and E7) across all treatment conditions;

2. Treatment_PUNA_vs_MEOH, comparing PunA-treated versus MeOH control samples across all cell lines;

3. PunA response interaction analysis, assessing differential transcriptional responses to PunA between HEYA8 and P201 cells by modeling the interaction between cell line and treatment.

2.14. Statistical Analysis

Cell viability was assessed using the MTS assay, comparing PunA treatment to methanol vehicle controls. Data are presented as mean ± standard deviation (SD). Statistical analyses were performed in GraphPad Prism. Depending on the experimental design, differences between groups were evaluated using paired t-tests, one-way ANOVA, or two-way ANOVA. Post hoc analyses were conducted with Tukey's multiple comparison test following paired t-tests and Dunnett's test following ANOVAs, with $p < 0.05$ considered statistically significant.

RNA sequencing was performed by Admera Health (South Plainfield, NJ, USA) using the Illumina platform. FastQC (v0.11.8) was used for quality control of raw sequencing data, and Trimmomatic (v0.38) was applied to remove adaptor sequences and trim low-quality bases. Sequencing reads were aligned to the reference genome using STAR Aligner (v2.7.1a), and duplicate reads were marked with Picard tools (v2.20.4). Differential expression and interaction analysis was performed to evaluate whether PunA induces differential transcriptional responses between HEYA8 (cancer) and P201 (normal) cells. The DESeq2 was applied to raw RNA-seq count data using a linear model including an interaction term: design = ~CellLine + Treatment + CellLine:Treatment where the

 doi:10.20944/preprints202602.0821.v1

interaction coefficient of 'CellLineHEYA8.TreatmentPunA' was quantified for the differences of (HEYA8PunA-HEYA8MEOH) – (p201PunA-p201MeOH). This $\log_2$ fold change (LFC) measures how much stronger the PunA-induced transcriptional changes is in HEYA8 relative to P201. LFC > 0 represents the PunA response is stronger in HEYA8 while LFC < 0 represents the PunA response is stronger in P201. Differential expression was assessed using a Wald test and adjusted for multiple testing using Benjamini–Hochberg FDR. Genes with $p_{adj} < 0.05$ were considered significant interaction genes. StringTie (v2.0.4) was employed for transcript assembly, and featureCounts (v1.6.0) or HTSeq was used to quantify reads mapped to genes, exons, promoters, gene bodies, genomic bins, and chromosomal regions. Differential expression analysis was performed using DESeq2 (v1.14.1), and Gene Ontology (GO terms) enrichment analysis was conducted with the ClusterProfiler package in R.

3. Results

3.1. Aging Promotes Tumor Expansion in Immunocompetent Mice

Previously, we found that OC development is more pronounced in aged RNU athymic nude rats [13], whose lack of a functional thymus and T cells render them severely immunodeficient in terms of cellular immunity. In the current study, we expanded upon these findings by examining OC progression in the C57BL/6 mouse model, a strain widely used in immunological research because of its robust immune response [26]. In this model, mouse ID8-OC cells were intraperitoneally inoculated into young (8 weeks) and aged (19 months) C57BL/6 mice. Bioluminescence imaging (IVIS) live imaging was performed on days 11 and 18 post-injection (Figure 1). Aged mice consistently exhibited stronger abdominal bioluminescence signals at both timepoints (Figure 1A). Quantitative IVIS measurements confirmed significantly higher total photon flux in aged mice compared to young controls at both 11- and 18-days post-injection (Figure 1B), indicating accelerated tumor growth and dissemination in older hosts like we have identified with the nude rats [13]. The longitudinal imaging demonstrated a progressive increase in tumor-associated photon flux across both cohorts. On day 11, aged mice showed a non-significant trend toward higher signal intensity relative to young mice ($p = 0.39$). By day 18, however, this difference reached statistical significance ($p = 0.03$), demonstrating that aging markedly enhances tumor expansion in this immunocompetent model.

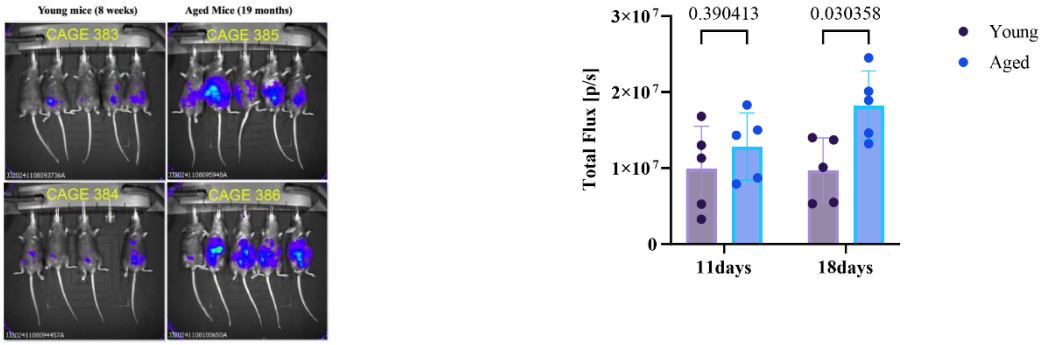

(**a**) (**b**)

Figure 1. Aged mice demonstrated a larger tumor burden compared to young mice. (**a**) In vivo bioluminescence imaging of tumor burden following intraperitoneal injection of ID8-OC cells into young (8-week-old) and aged (19-month-old) female C57BL/6 mice. Representative IVIS images were obtained on day 18 post cancer cell injection; (**b**) The total flux was measured for young (8-week-old) and aged (19-month-old) female C57BL/6 mice. The mean values of total flux were used for the comparison of tumor formation on day 11 and day 18 after OC cell injection. Quantification of total photon flux (p/s) revealed a trend toward higher tumor-associated signal in aged mice compared with young mice at day 11 ($p = 0.39$), with the difference becoming statistically significant at day 18 ($p = 0.03$).

 doi:10.20944/preprints202602.0821.v1

3.2. PunA Suppresses Cancer Progression in a Xenograft Mouse Model

In a previous study, we examined the dose-dependent cytotoxicity of PunA using OC cell lines A2780, HEYA8, and CAOV2, which suggested that FFAs may possess therapeutic potential in cancer prevention and treatment [13]. Building on these findings, we next evaluated PunA in an aged ID8-OC xenograft model using immunocompetent C57BL/6 mice. The effects of PunA ID8-OC cells were first assessed in vitro using concentrations ranging from 5 to 160 μM (Figure 2A). PunA reduced cell viability in a dose-dependent manner, with significant effects observed at concentrations ≥ 20 uM ($p < 0.05$). To test in vivo efficacy, young C57BL/6 mice were intraperitoneally injected with ID8-OC cells and, beginning on day 3 post-injection, treated daily with PunA (30 mg/mouse) for 3 weeks. Bioluminescence imaging at the end of treatment revealed that PunA-treated mice (n = 3) exhibited markedly reduced tumor-associated photon flux compared to the untreated control (n = 1) (Figure 2B). Although these data suggest that PunA may suppress OC progression in vivo, interpretation is limited by the small sample size and the lack of statistical analysis, primarily due to the use of only a single control mouse. Thus, validation in larger cohorts is needed to confirm the in vivo therapeutic potential of PunA.

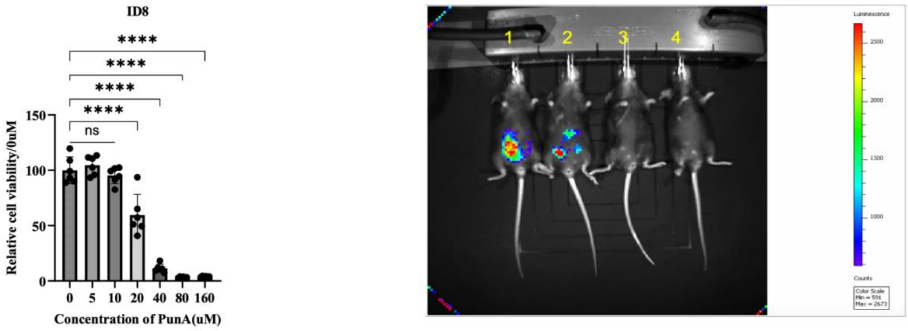

(**a**) (**b**)

Figure 2. Anti-tumor effects of PunA on mouse ID8 ovarian cancer cells in vitro and in vivo. (**a**) ID8 cells were treated with increasing concentrations of PunA (0–160 μM) for 48 hours, and cell viability was assessed by MTS assay. PunA reduced cell viability in a dose-dependent manner, with significant inhibition observed at concentrations ≥20 μM. Data are presented as mean ± SD. The test was performed with six repeats for each treatment condition; (**b**) Young (8-week-old) C57BL/6 mice were intraperitoneally injected with ID8-OC cells. From day 3 post-injection, mice received daily intraperitoneal administration of PunA (30 mg/mouse) for 3 weeks. In vivo bioluminescence imaging at end of week 3 of treatment is shown: mouse #1 represents the control group, while mice #2–4 represent the PunA-treated group. The PunA group displayed markedly reduced tumor-associated photon flux compared to the control.

3.3. PunA Induces Cancer-Specific Cell Death

Cisplatin has long been a first-line chemotherapeutic for OC patients, but its clinical use in long term treatment is limited by its toxicity to normal tissues [27]. To compare the cytotoxicity of PunA with cisplatin, HEYA8 OC cells and two immortalized NFT epithelial cell lines (P201 and P211) were treated for 48 hours with vehicle control (methanol), 20 μM PunA, 25 μM PunA, or 20 μM cisplatin (Figure 3A). MTS assay results revealed that PunA selectively reduced HEYA8 viability by >70% at both doses, while P201 and P211 viability was largely preserved. In contrast, cisplatin reduced viability by >70% in HEYA8 and caused even greater reductions in P201 and P211, confirming its non-selective cytotoxicity.

To further assess cancer selectivity, HEYA8 and four normal cells lines—P201, P211, mouse preadipocytes (3T3-L1) and normal ovarian epithelial cells (E7)—were exposed to increasing concentrations of PunA for 48 hours (Figure 3B). MTS assay results revealed

 doi:10.20944/preprints202602.0821.v1

PunA markedly reduced HEYA8 cell viability in a dose-dependent manner, with significant inhibition observed at concentrations ≥ 5 μM and near-complete loss of viability at 40 μM. In contrast, P201 and P211 exhibited only modest reductions in viability at higher doses, while 3T3-L1 and E7 cells remained largely unaffected across the tested range. Statistical comparison of nonlinear regression fits revealed significant differences between HEYA8 and P201 ($p = 0.027$), 3T3-L1 ($p = 0.007$), and E7 ($p = 0.007$), whereas the difference between HEYA8 and P211 was not significant ($p = 0.150$). These findings support PunA's selective toxicity toward OC cells.

Another member of omega-5 FFA 18:3 family, α-ESA, has very high structural similarity to PunA and is categorized as its geometric isomer (Figure 3C). To determine whether PunA's effects extend to α-ESA, HEYA8 and P201 cells were treated with increasing concentrations of each compound for 48 hours (Figure 3D). MTS assay results demonstrated that α-ESA reduced viability in both cancerous and normal cells, indicating non-selective toxicity. In contrast, PunA decreased HEYA8 viability in a dose-dependent manner while minimally affecting P201 cells. Summarized IC_{50} values for PunA (Figure 3E) further quantify this selectivity: normal cell lines consistently exhibited higher IC_{50} values (>40 μM), whereas OC cell lines displayed much lower IC_{50} values (~25 μM or even lower). The highly sensitive response of HEYA8 cells to PunA ($IC_{50} = 8.915$), is significant, as HEYA8 cells are derived from high-grade serous ovarian cancer (HGSOC), the most prevalent and aggressive epithelial OC histological subtype [28]. Additionally, CAOV2 cells exhibited a relatively sensitive response to PunA ($IC_{50} = 25.41$) compared to normal cell lines. This is notable given we previously found that CAOV2 cells, derived from OC ascites, exhibit chemoresistance to conventional chemotherapies under acidic conditions characteristic of the ascites TME [29]. Collectively, these results demonstrate that PunA preferentially targets OC cells while sparing normal counterparts, distinguishing it from α-ESA.

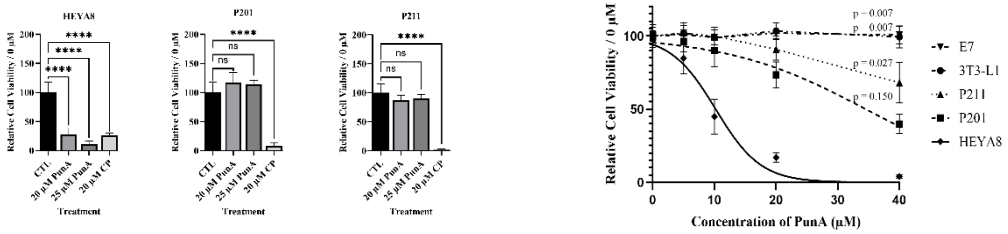

(a) (b)

Punicic Acid, ω-5	α-Eleostearic Acid, ω-5
9(Z),11(E),13(Z)-Octadecatrienoic Acid	9(Z),11(E),13(E)-Octadecatrienoic Acid
long-chain polyunsaturated fatty acid / conjugated trienoic fatty acid	long-chain polyunsaturated fatty acid / conjugated trienoic fatty acid
pomegranate seed oil	tung and bitter melon seed oil

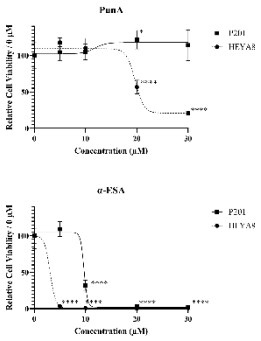

Cell Lines	Cell Line Origin	IC50 (μM)
E7	Scraped Normal Ovarian Epithelial Cells	>40
3T3-L1	Mouse Normal Preadipocytes	> 40
P201	Immortalized Human Fallopian Cells	43.08
P211	Immortalized Human Fallopian Cells	> 40
HEYA8	Epithelial Ovarian Cancer	8.915
A2780	Epithelial Ovarian Cancer	24.19
CAOV2	Epithelial Ovarian Cancer Ascites	25.41

(c) (d) (e)

Figure 3. Differential Effects of Punicic Acid and α-Eleostearic Acid on OC and Normal Cell Lines. (**a**) HEYA8 OC cells and NFT epithelial cell lines (P201 and P211) were treated for 48 h with methanol control (CTL, black bars), 20 μM PunA (medium grey bars), 25 μM PunA (dark grey bars) or 20 μM cisplatin (CP, light grey bars). PunA inhibited OC cell growth by > 70% at 20-25 μM, while NFT cell viability remained unaffected at the same concentrations. In contrast, cisplatin reduced viability in both cancerous and normal cells more than 65%. Data are presented as mean ± SD. Statistical significance was determined by one-way ANOVA with Tukey's post hoc

 doi:10.20944/preprints202602.0821.v1

test. ****p < 0.001, ns: not significant; (**b**) OC cells and normal cell lines were treated with increasing concentrations of PunA (0, 5, 10, 20, and 40 μM) for 48 h, and cell viability was determined by the MTS assay. Nonlinear regression curves are shown for HEYA8 and P201, which exhibited measurable dose-dependent responses. Non-responsive cell lines (P211, 3T3-L1, and E7) are displayed with straight line connections between data points. P-values indicate comparisons between each cell line and HEYA8. Data represent mean ± SD from three independent experiments. Statistical significance was evaluated by one-way ANOVA followed by Dunnett's post hoc test; (**c**) Structural comparison of PunA (cis-9, trans-11, cis-13) and α-ESA (cis-9, trans-11, trans-13), both conjugated trienoic FFAs differing only in the π-bond orientation at the omega-5 carbon; (**d**) HEYA8 and P201 cells were treated for 48 h with varying concentrations of PunA and α-ESA. While α-ESA reduced viability in both HEYA8 and P201 cells, PunA showed a dose-dependent reduction in HEYA8 viability with minimal cytotoxicity in P201 cells. Data are presented as mean ± SD of six replicates, representative of two independent experiments. Nonlinear regression curves are shown for HEYA8 and P201, and P-values indicate comparisons between treatment and control. Statistical significance was determined by two-way ANOVA with Dunnett's post hoc test. *p < 0.05, ****p < 0.0001; (**e**) Summary table of PunA IC_{50} values between normal cell lines (top four rows) and OC cell lines (bottom three lines).

3.4. PunA Enhances Chemosensitivity of OC Cells

Clinical use of platinum-based chemotherapeutics for OC treatment is limited by their toxicity to normal cells [30,31]. To determine whether combining PunA and cisplatin could preserve chemotherapeutic efficacy while mitigating cisplatin-associated toxicity, HEYA8 cells were treated for 48 hours with 20 μM PunA, 20 μM cisplatin, or their combination (Figure 4A). MTS assay results revealed that PunA alone reduced cell viability by 58%, while cisplatin alone reduced viability by 54%. The combination treatment produced a significantly greater reduction, decreasing viability by an additional 12% compared to PunA alone ($p < 0.05$) and 16% compared to cisplatin alone ($p < 0.01$). These results indicate that PunA enhances the chemosensitivity of OC cells to cisplatin, supporting the possibility that lower cisplatin doses could achieve equivalent or greater therapeutic effects when combined with PunA. Importantly, because PunA selectively spares normal cells, this strategy may reduce the dose-dependent cytotoxicity of cisplatin while preserving antitumor efficacy.

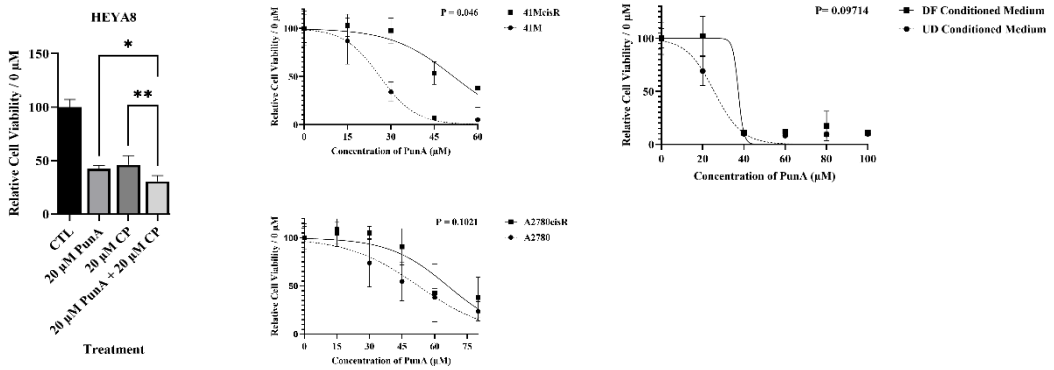

(**a**) (**b**) (**c**)

Figure 4. Synergistic Effects of Punicic Acid with Cisplatin, PunA Efficacy in Resistant Cells, and Impact of Lipidic Microenvironmental Conditions on PunA Activity. (**a**) HEYA8 cells were treated for 48 h with a methanol vehicle control, 20 μM PunA, 20 μM cisplatin, or a combination of 20 μM PunA and 20 μM cisplatin. Combination treatment reduced OC cell viability by 12% compared to cells treated with PunA alone and by 16% compared to cisplatin alone. Data are presented as mean ± SEM. Statistical significance was determined by one-way ANOVA with Tukey's post hoc test. *p < 0.05, **p < 0.01; (**b**) 41M/41McisR and A2780/A2780cisR cell pairs were treated for 48 h with PunA at concentrations ranging from 0 μM-60 μM for 41M pair (upper panel) and 0 μM-75 μM for A2780 pair (lower panel). At 60 μM PunA, PunA reduced viability by 95% reduction in 41M compared with 62% in 41McisR. At 75 μM, PunA reduced viability by 77% in A2780 compared with 62% in

 doi:10.20944/preprints202602.0821.v1

A2780cisR. Data are fitted by nonlinear regression and presented as mean ± SEM. Statistical significance was assessed using a two-tailed paired t-test; (**c**) HEYA8 cells were cultured in differentiated (DF) or undifferentiated 1 3T3-L1 conditioned medium and treated with increasing concentrations of PunA (0-100 μM) for 48 h. Cell viability was measured by MTS assay, normalized to untreated controls, and fitted by nonlinear regression. The cell viability appeared higher in DF-conditioned medium, particularly at PunA concentrations < 40 μM, although the differences were not statistically significant ($p = 0.097$). Data are presented as mean ± SEM, and statistical significance was evaluated by a two-tailed paired t-test.

3.5. Chemo-Resistant OC Cells Exhibit Diminished Sensitivity to PunA

An additional challenge in OC treatment is the frequent emergence of chemo-resistance, especially when long-term chemotherapy is applied [3]. To evaluate the effects of PunA in cisplatin-resistant OC cells, paired cisplatin-sensitive and resistant lines (41M/41McisR and A2780/A2780cisR) were treated with PunA at concentrations ranging from 0 μM to 75 μM increasing in 15 μM increments (Figure 4B). The data showed that PunA reduced cell viability in a dose-dependent manner; however, this efficacy was diminished in the cisplatin-resistant cells relative to their parental counterparts in both cell pairs. Our study showed that PunA did not display enhanced activity against cisplatin-resistant cells, suggesting that resistance mechanisms limit cancer cell response to PunA.

3.6. PunA Remains Effective in High Fat Environments

Next, we tested the sensitivity of PunA in OC cells cultured under a high-fat environment (Figure 4C), a common condition in both micro- and macro-environments in patients with OC [32]. 3T3-L1 preadipocytes were differentiated into adipocytes using a standard hormone cocktail, including insulin, which led to the accumulation of lipid droplets. This process is a well-established model for studying fat cell biology and adipogenesis33. Conditioned medium was collected from differentiated (DF) and undifferentiated (UD) 3T3-L1 cultures and used to mimic fatty versus non-fatty conditions, respectively. HEYA8 cells were then treated with PunA at 0-100 μM in 20 μM increments under both DF- and UD-conditioned media. PunA reduced cell viability in a dose-dependent manner, but no statistically significant differences were observed between the fatty and non-fatty conditions. These results indicate that PunA retains similar anticancer activity even under high-fat conditions.

3.7. PunA Triggers Ferroptosis

Many lipid-derived factors, particularly FFAs, exert cytotoxic effects by inducing ferroptosis, an iron-dependent, non-apoptotic form of cell death triggered by lipid peroxidation34. To determine whether ferroptosis mediates PunA-induced cell death, HEYA8 and A2780 cells were co-treated with PunA and 2 μM Ferrostatin-1 (Fer-1), a potent, synthetic inhibitor of ferroptosis (Figure 5A). PunA alone reduced viability by 93% in HEYA8 cells and 97% in A2780 cells, whereas co-treatment with Fer-1 significantly rescued viability ($p < 0.001$). These findings indicate that ferroptosis plays a key role in PunA-induced cytotoxicity in OC cells. To further validate this mechanism, RT-qPCR was performed in HEYA8 cells treated with 25 μM PunA for 48 hours (Figure 5B). PunA significantly increased RNA expression of ferroptosis markers SLC7A11 ($p = 0.003$) and CHAC1 ($p = 0.023$) compared with the vehicle control (methanol) by 40% and by 15%, respectively. Taken together, these findings support the involvement of ferroptosis in PunA-induced OC cell death.

 doi:10.20944/preprints202602.0821.v1

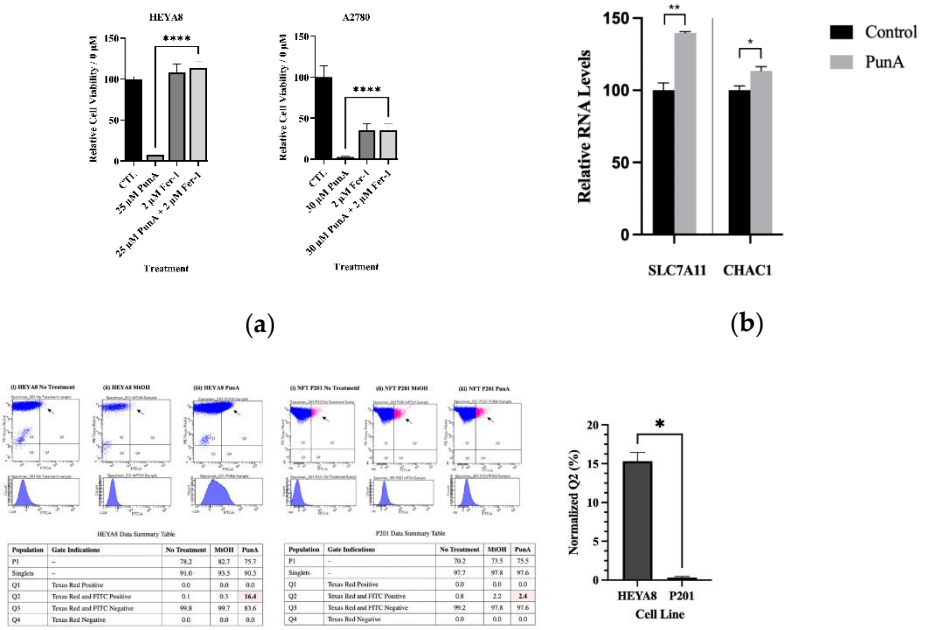

Figure 5. PunA induces OC cell ferroptosis and lipid peroxidation. (**a**) HEYA8 cells and A2780 cells were treated with PunA (25 μM for HEYA8 and or 30 μM for A2780), 2 μM of Fer-1, and the combination of Fer-1 and PunA for 48 h. The cell viability was tested using MTS assay. Data is presented as mean ± SEM. Statistical significance was determined by one-way ANOVA with Tukey's post hoc test. ****$p < 0.0001$; (**b**) HEYA8 cells were treated with 25 μM PunA or mock treatment control (methanol) for 48 h. The expression for genes SLC7A11 and CHAC1 was performed using RT-qPCR. The SLC7A11 and CHAC1 RNA levels were significantly higher in HEYA8 cells treated with PunA ($p = 0.003$ and $p = 0.023$, respectively) compared to the methanol mock treatment control. Data is presented as mean ± SEM. Statistical significance was determined by paired t test. *$p < 0.05$, **$p<0.01$; (**c**) BODIPY 581/591 C11 staining and flow cytometry analysis were performed on HEYA8 and P201 cells after the cells were untreated (left panel), treated with methanol (MtOH, middle panel), or 10 μM of PunA (right panel) for 24 h. Q1 showed the percentage of cells that were Texas Red single positive, Q2 was Texas Red and FITC double positive, Q3 was Texas Red and FITC double negative, and Q4 was FITC single positive for each of the treatment types. HEYA8 cells show a noticeable shift from Q1 to Q2 compared to the control and methanol vehicle control groups while P201 cells show a negligible shift, indicating a greater percentage of HEYA8 cells undergoing PunA induced lipid peroxidation. Percentage of Q2-positive (Texas Red and FITC double-positive) cells, reflecting oxidized lipid accumulation measured by BODIPY 581/591 C11 staining. Percentage values represent PunA-treated cells after subtracting their respective methanol controls to account for methanol vehicle control. The bar graph was generated from two independent tests and is presented as mean ± SEM. Statistical significance was determined by paired t-test. *$p < 0.05$.

3.8. PunA Selectively Increases Lipid Peroxidation in OC Cells

Ferroptosis and lipid peroxidation are tightly linked, with iron-dependent lipid peroxidation serving as a key driver ferroptosis [35,36]. To determine whether PunA selectively induces lipid peroxidation in OC versus NFT cells, HEYA8 and P201 cells were treated with vehicle control (methanol) or 10 μM PunA for 24 hours, followed by BODIPY 581/591 C11 staining and flow cytometry (Figure 5C). The Q2 population, representing the double-positive for both Texas Red and FITC, reflects cells undergoing lipid peroxidation.

Methanol (MtOH) controls produced minimal shifts in fluorescence, confirming low baseline oxidation stress. In contrast, PunA treatment dramatically increased lipid peroxidation in HEYA8 cells (16.4% Q-positive), while only a minimal increase was observed in P201 cells (2.4%). After normalization to their respective methanol controls, PunA treatment resulted in a net 16.1% increase

 doi:10.20944/preprints202602.0821.v1

in lipid peroxidation in HEYA8 cells versus only 0.2% in the P201 cells (Figure 5C). These results demonstrate that PunA selectively induces lipid peroxidation in OC cells but not in normal cells, supporting a model in which PunA selectively triggers ferroptosis through lipid peroxide accumulation in cancer cells.

3.9. PunA Selectively Upregulates PPAR-γ Activity in OC Cells

Given the differential sensitivity of OC and NFT cells to PunA, we next examined the expression of Peroxisome Proliferator-Activated Receptor gamma (PPAR-γ) in HEYA8 and P201 cells (Figure 6A). PPAR-γ is a transcription factor that plays a central role in lipid metabolism, cell proliferation, and carcinogenesis [37]. PunA significantly upregulated PPAR-γ expression in HEYA8 cells in a dose-dependent manner, with a significant increase observed at 60 μM PunA ($p = 0.0023$). In contrast, PunA did not induce significant changes in PPAR-γ levels in P201 cells at any concentration, suggesting a cell-type-specific regulation of PPAR-γ by PunA.

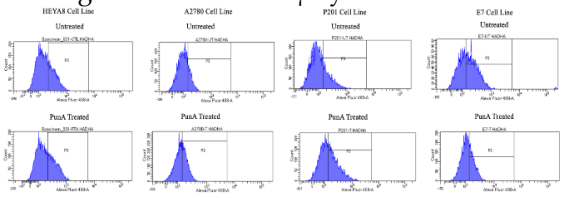

Cell Line	Treatment	P3 Fluorescence (% of Parent Population)	Difference
HEYA8	Control (MtOH)	31.0%	5.1%
	PunA	36.1%	
A2780	Control (MtOH)	19.8%	19.9%
	PunA	39.7%	
P201	Control (MtOH)	37.6%	-14.6%
	PunA	23.0%	
E7	Control (MtOH)	52.6%	-19.1%
	PunA	33.5%	

(**b**)

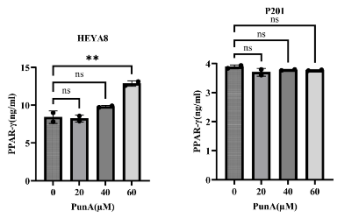

(**a**)

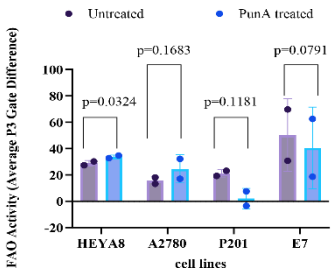

(**c**)

Figure 6. PPAR gamma and Fatty Acid Oxidation showed differential activities in cancer cells and noncancerous cells. (**a**) PunA induced PPAR-γ activity in HEYA8 at 60 μM ($p=0.0023$) but not in P201 cells. HEYA8 (left) and P201 (right) cells were treated with increasing concentrations of PunA (0, 20, 40, and 60 μM) for 24 h. PPAR-γ activities were measured using an ELISA kit. Data is presented as mean ± SEM from three independent experiments. Statistical analysis was performed using one-way ANOVA with Tukey's post hoc test. $p < 0.01$; ns: not significant; (**b**) Fatty Acid Oxidation (FAO) activity levels were examined by HADHA expression in cancer cell lines, HEYA8 and A2780, and noncancerous cell lines, P201 and E7, following PunA treatment. Flow

 doi:10.20944/preprints202602.0821.v1

cytometry analysis was used to analyze the HADHA expression which is shown in gate P3. This initial representation (without IgG control comparison) demonstrates the difference between the control (MtOH) and PunA treatment groups. Fluorescence in the P3 gate increased in cancerous cell lines and decreased in noncancerous cell lines between control and treatment groups; (**c**) Average FAO activity from two independent tests showed HADHA expression increasing in HEYA8 and A2780 cell lines with 10 μM PunA and 25 μM PunA respectively, compared to untreated groups. Average HADHA expressions decreased in noncancerous cell lines, P201 and E7, with 25 μM of PunA treatment compared to untreated groups. Statistical analysis was performed using a two-tailed paired student t-test with $p < 0.05$ considered significant for HADHA expressions (population percentage of gate 3). .

3.10. PunA Induces Differential Fatty Acid Oxidation Activity

Fatty acid oxidation (FAO) is the primary metabolic pathway for generating cellular energy from fatty acids, a process that occurs primarily in the mitochondria [38]. FAO plays a multifaceted role in cancer by supplying energy that supports tumor growth, metastasis, stemness, and drug resistance in both cancer cells and the tumor microenvironment [38]. The hydroxyacyl-CoA dehydrogenase trifunctional multienzyme complex subunit alpha (HADHA) gene encodes a key mitochondrial enzyme complex that directly regulates the rate of FAO [39].

To assess how PunA affects FAO in PunA-treated OC and NFT cells, we first verified whether the FAO-related genes included in the assay kit (ACADVL, ACADM, and HADHA) were expressed in the OC cells HEYA8 and A2780. Flow cytometry analysis revealed detectable expression of only HADHA (data not shown). After confirming HADHA expression in OC cells, we next quantified its expression following PunA treatment in four cell lines: HEYA8, A2780, P201, and E7. Flow cytometry analysis revealed distinct differences in HADHA expression between the OC cell lines (HEYA8 and A2780) and noncancerous epithelial cell lines (P201 and E7), as determined by P3 gating (Figure 6B). Data from two independent experiments are summarized in Figure 6C.

In both OC cell lines, PunA treatment increased HADHA expression, as evidenced by a higher percentage of cells within the P3 gate after correction for IgG control background. In HEYA8 cells, the proportion of cells in the P3 region increased significantly from an average of 28.85% in untreated cells to 33.75% following treatment with 10 μM of PunA ($p = 0.03$). A similar upward trend was observed in A2780 cells, where the proportion of cells in the P3 region rose from 15.65% in untreated cells to 24.55% after 25 μM PunA treatment. Although the increase in A2780 cells did not reach statistical significance ($p = 0.17$), the consistent elevation across both experiments supports a PunA-induced upregulation of HADHA in OC cells. In contrast, treatment of the noncancerous cell lines decreased the proportion of P3 cells, indicating reduced HADHA expression and, consequently, diminished FAO activity. In P201 cells, the P3 proportion declined from 21.15% in untreated cells to 2.00% after treatment with 25 μM PunA ($p = 0.12$), while E7 cells showed a reduction from 50.20% to 40.55% under the same conditions ($p = 0.08$). Although these changes did not reach statistical significance in every cell line, the consistent trend across experiments supports the hypothesis that PunA stimulates FAO in OC cells while repressing it in noncancerous epithelial cells.

3.11. PunA Selectively Impairs Mitochondrial Respiration in OC Cells

Given the importance of mitochondria in regulating lipid metabolism, we next assessed mitochondrial function using the Seahorse XF Cell Mito Stress Test. Treatment with PunA significantly suppressed mitochondrial respiration in HEYA8 cells in a dose-dependent manner (Figure 7A). As shown in the mitochondrial stress test, PunA notably reduced oxygen consumption rate (OCR) at all stages, particularly at higher concentrations (40 and 60 uM), indicating impaired mitochondrial function. Quantification of key parameters revealed marked decreases in basal respiration, maximal respiration, ATP production, and spare respiratory capacity in HEYA8 cells, with the most significant reductions observed at 60 uM PunA (Figure 7B). In contrast, P201 cells exhibited minimal or no significant changes in these parameters across all treatment groups (Figure

 doi:10.20944/preprints202602.0821.v1

7C), suggesting that PunA selectively impairs mitochondrial respiration in tumor cells but not in normal fallopian tube epithelial cells.

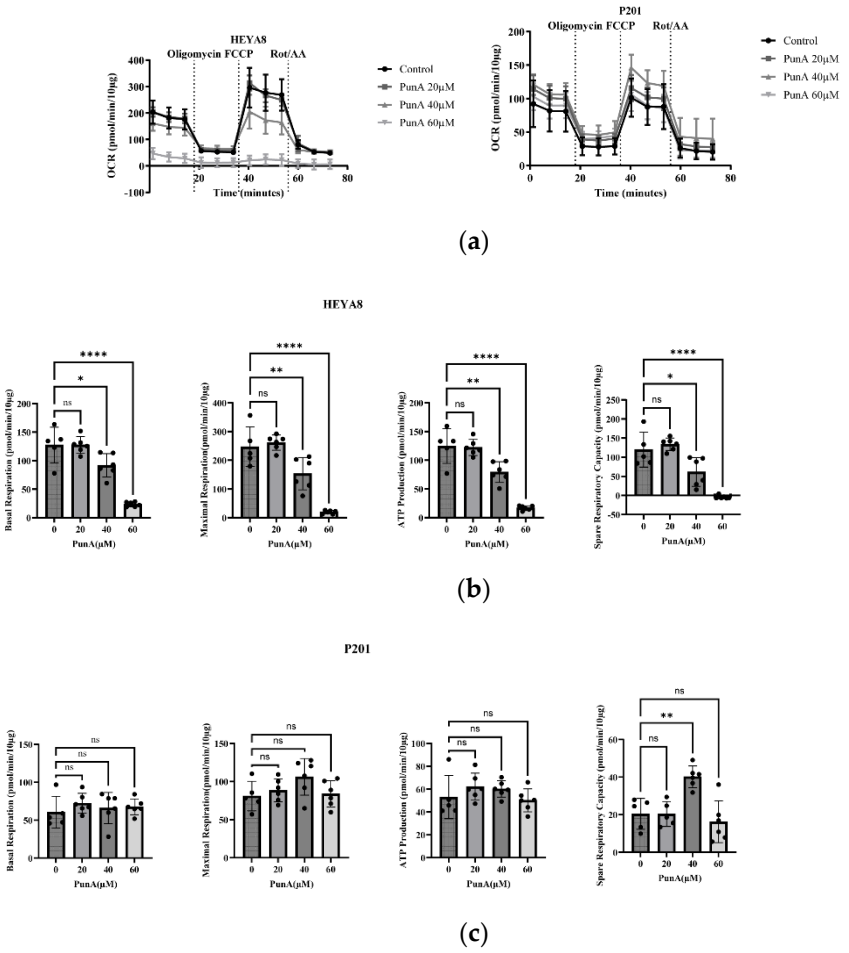

Figure 7. Differential effects of PunA on mitochondrial respiration in OC versus normal cells. (**a**) Oxygen consumption rate (OCR) profiles of OC HEYA8 (left) and NFT P201 (right) cells treated with different concentrations of PunA (20, 40, and 60 μM), assessed by Seahorse XF Mito Stress Test. Oligomycin, carbonyl cyanide-4-(trifluoromethoxy)phenylhydrazone (FCCP), and Rotenone/Antimycin A (Rot/AA) were sequentially injected at indicated time points; (**b-c**) Quantification of basal respiration, maximal respiration, ATP production, and spare respiratory capacity in HEYA8 (**b**) and P201 (**c**) cells. Data are presented as mean ± SEM. Statistical significance was determined by one-way ANOVA with Tukey's post hoc test. *$p < 0.05$, **$p < 0.01$, ***$p < 0.001$, ****$p < 0.0001$, ns: not significant.

3.12. PunA Alters Gene Expression and Pathway Activation

To investigate PunA-induced transcriptional changes, RNA-seq was conducted on OC cells (HEYA8 and A2780) and normal epithelial cells (P201 and E7), under both PunA-treated and control (methanol) conditions. A total of 78,932 transcripts were analyzed (Table S1), and principal component analysis (PCA) was performed to assess gene expression profiles (Figure 8A). The PCA revealed clear separation among all samples in the score plot, with tight clustering within groups of cancer and normal cells, indicating distinct transcriptional profiles between OC and normal epithelial cells, as well as between PunA-treated OC and PunA-treated normal cells. Using the thresholds of $|\log2FC| \geq 1$ and $p_{adj} \leq 0.05$, we identified 7,038 differentially expressed genes (DEGs) between the OC and the normal epithelial cell lines across treatment conditions. The distribution of these DEGs is presented in the volcano plot (Figure 8B), and the heatmap of the top 100 DEGs (Figure 8C) clearly distinguishes cancerous from normal samples.

 doi:10.20944/preprints202602.0821.v1

In contrast, a comparison of PunA-treated versus methanol (MtOH) control samples across all cell lines revealed 396 DEGs (Figure 8D). The top PunA-responsive DEGs are presented in the heatmap (Figure 8E), illustrating shared transcriptional alterations induced by PunA in both cancerous and non-cancerous cell lines.

In the cancer-versus-normal comparison, most DEGs were protein-coding genes, including *MMP2*, *COL1A1*, *CXCL5*, and *CDH11*, which are strongly associated with extracellular matrix remodeling, immune regulation, and tumor progression. Several DEGs were also linked to adipokine signaling and lipid metabolism, such as *FABP5*, *LPAR3*, *P2RX7*, *MMP2*, *COL1A1*, and *CXCL5*. In contrast, PunA-responsive DEGs were predominantly pseudogenes, long non-coding RNAs (lncRNAs), and unannotated transcripts (e.g., *LINC01842*, *MIR563*, *RNU5D*-1), with relatively fewer protein-coding genes identified. Notably, these PunA-associated transcripts showed limited evidence of direct involvement in adipokine pathways based on current literature [40–42].

Next, KEGG pathway and Gene Ontology (GO) enrichment analyses were performed on DEGs from both comparisons (Table S2, Table S3). Using the selection criteria of $|NES| \geq 1$ and $p \leq 0.05$, we identified significant enrichment across 48 KEGG pathways, 728 biological processes (BP), 76 molecular functions (MF), and 70 cellular components (CC). Several pathways—including cytokine–cytokine receptor interaction, PI3K–Akt signaling, human papillomavirus infection, cytoskeleton regulation, calcium signaling, herpes simplex virus 1 infection, and cell adhesion molecules—were enriched in both comparisons. In other words, these pathways were upregulated in OC cells compared to normal cells and again upregulated in PunA-treated OC cells relative to untreated cells. GO biological processes further highlighted extracellular matrix organization, response to virus, leukocyte migration, cell–cell adhesion, and collagen metabolic processes. Collectively, these results indicate that the DEGs are significantly enriched in pathways related to immune regulation, metabolism, infection response, and tumor-associated signaling processes.

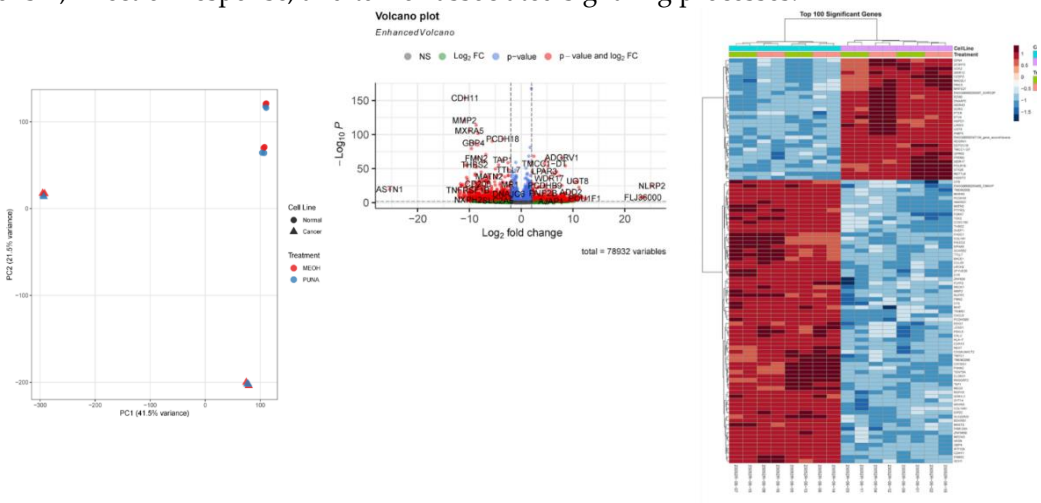

(**a**) (**b**) (**c**)

 doi:10.20944/preprints202602.0821.v1

(**d**) (**e**) (**f**)

Figure 8. Transcriptomic profiling of PunA treatment in ovarian cancer and normal cells. (**a**) Principal component analysis (PCA) of RNA-seq data from cancer cells (HEYA8 and A2780 shown with triangle) and normal cells (P201 and E7 shown with dots). Samples were grouped by treatment with PunA in blue or methanol (MtOH) vehicle control in red. PCA clearly separated cancer and normal cells along the first principal component; (**b**) Volcano plot showing differentially expressed genes (DEGs) between cancer and normal cell lines across all treatment conditions. Red and blue dots represent significantly up- and down-regulated genes, respectively ($|\log_2$ fold change$| \geq$, $p_{adj} < 0.05$); (**c**) Heatmap showing the top 100 differentially expressed genes between cancer cell lines (A2780 and HEYA8) and normal cell lines (P201 and E7) across all treatment conditions. Distinct expression profiles separate cancerous (pink) from normal (light blue) samples. Blue indicates down-regulated genes and red indicates up-regulated genes, with color intensity reflecting the magnitude of expression change; (**d**) Volcano plot showing differentially expressed genes (DEGs) between PunA-treated and MeOH control samples across all cell lines. Red and blue dots represent significantly up- and down-regulated genes, respectively ($|\log_2$ fold change$| \geq 1$, $p_{adj} < 0.05$); (**e**) Heatmap showing the top differentially expressed genes between PunA-treated and MeOH control samples across all cell lines. PunA treatment substantially altered global gene expression patterns, demonstrating its overall transcriptional impact on both cancer (A2780, HEYA8) and normal (P201, E7) cell lines. Red and blue denote up- and down-regulated genes, respectively, with color intensity reflecting expression magnitude; (**f**) KEGG pathway enrichment analysis was performed separately on DEGs identified from the Cancer_vs_Normal comparison and the PunA_vs_MeOH treatment comparison. Several pathways, including cytokine–cytokine receptor interaction, PI3K–Akt signaling, human papillomavirus infection, cytoskeleton regulation, and calcium signaling, were enriched in both analyses. The overlap suggests that these pathways may contribute not only to the intrinsic differences between cancer and normal cells but also to the global transcriptional response induced by PunA treatment.

3.13. PunA Enhances Inflammatory and Immune Gene Expression in OC Cells

To assess cell-type-specific transcriptional sensitivity to PunA, we quantified the differential gene expression responses between HEYA8 OC and P201 normal epithelial cells (Figure 9A). Among 29,843 genes analyzed, 588 genes (2%) exhibited significantly stronger PunA-induced responses in HEYA8 cells, whereas 306 genes (1%) showed greater responsiveness in P201 cells (Table S4). This asymmetric distribution indicates that the overall transcriptional impact of PunA is biased toward activation in HEYA8 cancer cells. As part of RNA-seq processing, low-count genes were removed by independent filtering, consistent with standard analysis workflows. Notably, several major interaction genes—including *CXCL8*, *GREM1*, *MMP1*, *SQSTM1*, *HSPA1B*, and *C1S*—displayed large response differences ($\log_2$FC = 1.4–4.0, $p_{adj} = 10^{-57}$ to 10^{-161}). These genes are associated with inflammation, extracellular matrix remodeling, stress responses, and immune regulation, suggesting that PunA activates a more robust inflammation- and stress-related transcriptional program in HEYA8 cells.

 doi:10.20944/preprints202602.0821.v1

PCA analysis (Figure 9B) revealed clear separation between PunA-treated and control samples in both HEYA8 and P201 cells, indicating transcriptional responsiveness in both. However, the heatmap of the top 100 PunA-responsive genes (Figure 9C) showed markedly greater expression changes in HEYA8 cells, reinforcing cell-type-specific transcriptional effects. The volcano plot (Figure 9D) further highlighted genes strongly upregulated in HEYA8, such as *CXCL8*, *GREM1*, *MMP1*, *SQSTM1*, *HSPA1B*, and *C1S*.

To explore the functional implications of these transcriptional differences, KEGG and Gene Ontology (GO) enrichment analyses were conducted using $|NES| \geq 1$ and $p \leq 0.05$ as significance criteria. We identified 18 KEGG pathways, 258 biological processes (BP), 6 molecular functions (MF), and 6 cellular components (CC) that were significantly enriched (Tables S5 and S6). Notable KEGG pathways included lipid and atherosclerosis, rheumatoid arthritis, amoebiasis, alcoholic liver disease, transcriptional misregulation in cancer, COVID-19, Legionellosis, TNF signaling, complement and coagulation cascades, IL-17 signaling, hematopoietic cell lineage, and NF-κB signaling. Enriched GO biological processes encompassed responses to bacterial molecules, response to lipopolysaccharide, regulation of immune effector processes, ECM organization, and cellular response to biotic stimulus. Collectively, these findings suggest that PunA modulates key inflammatory, immune, and tumor-associated pathways, eliciting a stronger transcriptional response in OC cells than in normal epithelial cells.

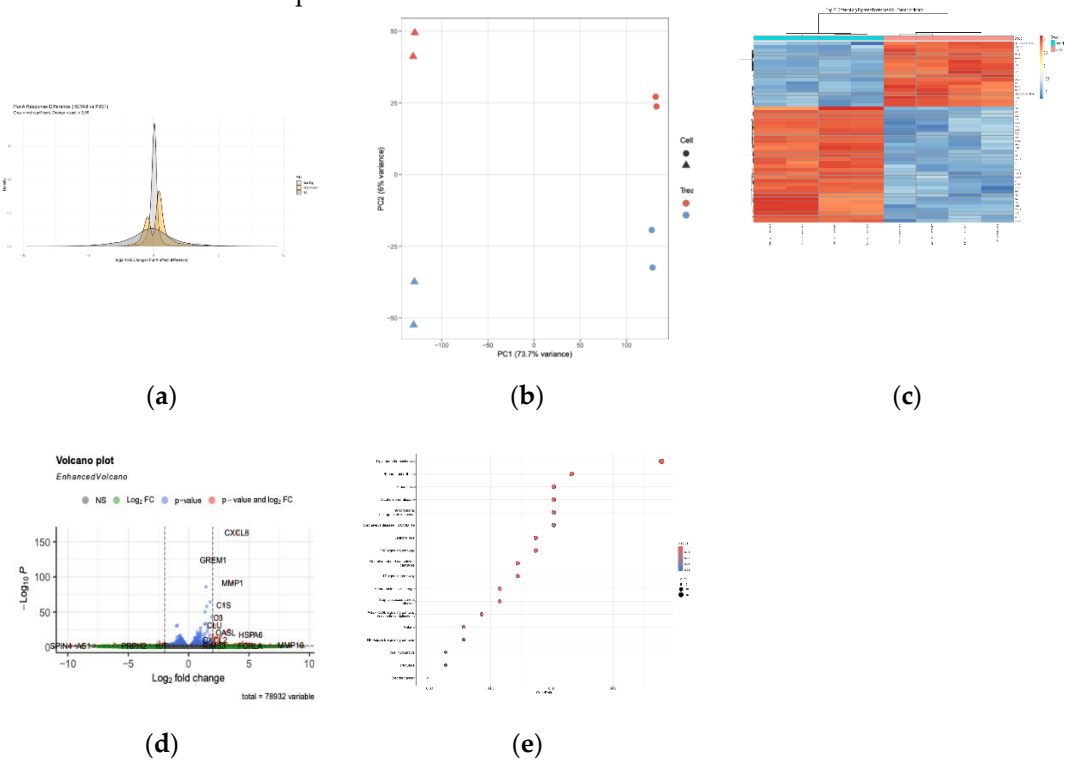

Figure 9. Transcriptomic analysis in HEYA8 versus P201 cells. (**a**) RNA-seq was performed on HEYA8 ovarian cancer cells and P201 immortalized human fallopian tube epithelial cells treated with PunA or MeOH (control). The density plot illustrates that HEYA8 ovarian cancer cells exhibit a stronger transcriptional response to PunA than the normal fallopian tube cells P201, as reflected by the distribution of $\log_2$ fold-change differences (HEY-A8 minus P201), with significant genes ($p_{adj} < 0.05$) highlighted in orange and the red dashed line indicating zero effect difference; (**b**) Principal component analysis (PCA) showing distinct clustering of samples according to treatment and cell line; (**c**) The heatmap illustrates distinct transcriptional responses to PunA between HEYA8 ovarian cancer cells and P201 normal fallopian tube cells. Gene expression values were scaled across samples, with red indicating higher expression and blue indicating lower expression. Hierarchical clustering of both genes and samples reveals that PunA induces a markedly stronger transcriptional shift in HEYA8 compared to P201, as evidenced by the formation of PunA-responsive gene clusters that segregate specifically in the HEYA8 samples. These patterns highlight cell-type-specific sensitivity to PunA treatment; (**d**) Volcano plot illustrating

 doi:10.20944/preprints202602.0821.v1

the differential transcriptional response to PunA between HEYA8 ovarian cancer cells and P201 normal fallopian tube cells. The x-axis represents the difference in PunA-induced $\log_2$ fold change between the two cell lines (HEYA8 – P201), such that positive values indicate genes with a stronger PunA response in HEYA8, while negative values indicate a stronger response in P201. Significantly differentially responsive genes are highlighted in red, with the top 10 most significant interaction genes labeled. The plot reveals that HEYA8 exhibits a markedly stronger transcriptional response to PunA compared with P201; (**e)** The bubble plot shows the top enriched KEGG pathways, with the bubble size representing the number of enriched genes and the color indicating the adjusted P-value. The enriched pathways are mainly related to inflammation, immune regulation, infection, and tumor-associated signaling processes.

4. Discussion

Our main findings in this study are as follows: the omega-5 fatty acid, PunA, inhibits ovarian cancer cell growth in vitro and may exert similar effects in vivo. PunA selectively targeted the malignant cells while sparing the normal epithelial cells, suggesting that PunA possesses cancer-specific activity. Through multiple mechanistic studies, we further found that PunA's cancer-specific chemotherapeutic effects are mediated by the regulation of PPAR-γ, FAO activity, mitochondrial dysfunction, and the modulation of multiple genes and pathways involved in remodeling key cell signaling pathways and immune-related programs. This study uniquely suggests that PunA could be developed as a cancer-specific chemotherapeutic agent that acts by inducing ferroptosis in cancer cells. Further studies, including clinical trials, are encouraged to facilitate the use of this agent in OC patients.

In our previous study [13] using the immunodeficient RNU rat model, we found that aged animals were more susceptible to OC development and displayed downregulation of multiple FFAs in tumor-surrounding AT, with PunA exhibiting the greatest reduction. In the current study, we extended these findings to an immune-competent system using the C57BL/6 mouse model, whose defined genetic background and major histocompatibility complex (MHC) haplotype make it ideal for investigating innate and adaptive immune responses [26]. In this system, aged hosts again supported greater tumor growth and expansion than younger mice (Figure 1). We also observed that PunA inhibited OC tumor progression in the C57BL/6 model, although interpretation was limited by small sample size (Figure 2). In vitro, PunA selectively reduced the viability of OC cells while sparing NFT epithelial cells, whereas its structural isomer α-ESA was broadly cytotoxic to both cancerous and normal cells (Figure 3). To our knowledge, this is the first report of PunA's selective anticancer effect in OC. Because NFT cells are believed to give rise to the majority (>80%) of HGSOC—the most common and most lethal subtype of OC [43]—this selective cytotoxicity is highly relevant for therapeutic development, as many standard chemotherapeutics cause significant off-target effects that limit their clinical utility [44]. Together with previous studies by several researchers showing that PunA kills breast cancer cells [18,19], our results emphasize the importance and safety of using PunA for patients with OC. Further animal studies and clinical trials are needed to identify its potential as a therapeutic agent in OC treatment.

The distinct toxicity profiles of PunA and its isomer α-ESA underscore the importance of stereochemistry in dictating biological activity. A plausible explanation for their divergent effects is that the two FFAs are metabolized and incorporated differently into cellular membranes. Compared to NFT cells, OC cells typically express higher levels of acyl-CoA synthetase long-chain family member 4 (ACSL4) [45], an enzyme that esterifies polyunsaturated fatty acids into phospholipids [46]. The 13-cis bond geometry of PunA may make it a preferred substrate for ACSL4, thus making it more likely to be incorporated into the phospholipid bilayer. Once integrated into the bilayer, PunA-containing phospholipids become highly susceptible to lipid peroxidation, a process that can compromise membrane integrity and promote cell death [47]. In contrast, the 13-trans configuration of α-ESA may reduce its suitability as an ACSL4 substrate, limiting its incorporation into membrane phospholipids. Without efficient integration, α-ESA would generate far less oxidative membrane

 doi:10.20944/preprints202602.0821.v1

damage and is more likely to initiate a more general, non-selective cell death mechanism, such as apoptosis. This theory fits the observed selectivity: When treated with PunA, OC cells, with higher ACSL4 levels, are more vulnerable to lipid-peroxide-mediated toxicity, whereas normal cells, with lower ACSL4 expression, remain resistant. Additional work is needed to confirm this proposed pathway.

PunA's ability to promote lipid peroxidation aligns with existing evidence that it induces ferroptosis, an iron-dependent form of cell death characterized by peroxide accumulation [48]. Because ferroptosis occurs through a mechanism distinct from first-line platinum-based agents such as cisplatin [48,49], we hypothesized that PunA could enhance cisplatin efficacy. Our results support this idea, as PunA appeared to synergize with cisplatin to produce a greater overall anticancer effect than either agent alone (Figure 4A). Here, "synergy" is defined in accordance with the Highest Single Agent model, as the combined effect exceeded that of the most potent individual compound [50]. These findings suggest that PunA-cisplatin co-treatment may enable cisplatin dose reduction while maintaining therapeutic potency. Such a strategy could prove critically important in mitigating chemotherapy-related toxicity and improving overall treatment tolerability. Animal studies should be conducted to further evaluate the combinative potential.

Given the promising results from combination treatment and PunA's distinct mechanism, we next asked whether PunA could also kill cisplatin-resistant (cisR) cells. Because resistance to platinum-based therapy is common in OC patients [51], determining whether PunA retains activity in this context is highly relevant. MTS assays in parental and cisR cell pairs of 41M and A2780 showed that PunA reduced viability in both groups, although parental cells were consistently more sensitive (Figure 4B). Thus, while PunA retains some activity in cisR cells at higher doses, its effects do not exceed those observed in cisplatin-sensitive cells. These findings suggest that PunA is unlikely to serve as an effective standalone treatment for cisplatin-resistant OC, though it may still hold value in combination strategies.

Another major clinical challenge in OC is metastatic spread. OC tumors frequently colonize the omentum, a large abdominal fat pad, and this process is driven by interactions between cancer cells and adipocytes [52]. Disrupting these cancer-fat cell interactions can therefore inhibit metastatic progression [53]. To determine whether PunA' activity is influenced by a fat-rich environment, we cultured HEYA8 cells in fat-enriched medium obtained by differentiating 3T3-L1 cells into adipocytes and assessed their response to PunA (Figure 4C). Viability was compared with HEYA8 cells grown in UD (fat-poor) medium. PunA reduced viability in a dose-dependent manner under both conditions, with no statistically significant differences between them. These findings indicate that PunA's anticancer activity is not diminished by adipose-rich environments, suggesting that it may remain effective within the omental microenvironment where OC commonly metastasizes.

After establishing PunA's selective anticancer activity, synergy with cisplatin, and efficacy across different microenvironmental conditions, we next sought to confirm whether ferroptosis is the central mechanism by which PunA acts in OC. Our mechanistic studies indicated that PunA induces ferroptosis in OC cells, because Fer-1, a ferroptosis inhibitor, rescued cell viability and counteracted PunA treatment (Figure 5A). Consistent with this observation, PunA treatment also increased the expression of established ferroptosis-associated markers, including SLC7A11 and Chac1, in OC cells (Figure 5B). Together, these data support the conclusion that PunA promotes OC cell death through ferroptosis, revealing a potential lipid-metabolic vulnerability that could be therapeutically exploited.

As previously mentioned, ferroptosis is defined by iron-dependent accumulation of lipid peroxides [48], distinguishing it from apoptosis and other forms of regulated cell death [54]. PunA is highly prone to oxidation due to its conjugated double-bond structure [36], so we tested whether its anticancer activity is linked to the induction of lipid peroxidation. Using the BODIPY 581/591 C11 probe, we observed a pronounced red-to-green fluorescence shift in HEYA8 cells following PunA treatment, with a net 16.1% increase in Q-positive cells, reflecting substantial oxidized lipid accumulation (Figure 5C). In contrast, the P201 cells showed only a net increase in Q-positive cells of

 doi:10.20944/preprints202602.0821.v1

0.2%, reflecting very low levels of oxidized lipids (Figure 5C). No such oxidative effects were observed in untreated or vehicle (methanol) treated controls, indicating that these changes were PunA-specific. These findings further support our model that PunA becomes incorporated into cancer cell membrane phospholipids, likely via the ACSL4-dependent pathway discussed earlier, where its highly oxidizable structure renders membranes vulnerable to iron-driven lipid peroxidation and subsequent ferroptosis [36]. This mechanism is particularly relevant in OC and other aggressive cancers where apoptosis resistance limits the effectiveness of standard therapies. Collectively, these data demonstrate that PunA selectively induces ferroptosis via lipid peroxidation in OC cells but not in normal cells, providing a coherent mechanistic base for its selective cytotoxicity.

We next investigated whether PunA also engages metabolic regulators that could contribute to this specificity. We focused on PPAR-γ, a lipid-sensing nuclear receptor implicated in metabolic control and tumor suppression [55]. PunA upregulated PPAR-γ expression in HEYA8 cells in a dose-dependent manner, whereas P201 cells showed no measurable changes even at the highest dose, indicating again a cancer-specific response (Figure 6A). PPAR-γ plays key roles in lipid handling, mitochondrial metabolism, and adipogenesis [55], and it is aberrantly expressed in several human cancers [56]. Its activation has been associated with growth inhibition, differentiation, and apoptosis [56]. Additionally, treatment with certain fatty acids, such as omega-3's, has been shown to suppress tumor growth while increasing PPAR-γ expression [57]. These observations raise the possibility that PunA may act, at least in part, through PPAR-γ activation, altering lipid homeostasis in a way that enhances susceptibility to ferroptosis. This is consistent with prior evidence that PPAR-γ regulates genes involved in proliferation and inflammation [58], providing a plausible transcriptional link between PunA treatment and an anticancer phenotype.

However, PPAR-γ's effects are highly ligand-dependent, and some synthetic ligands suppress OC proliferation through PPAR-γ-independent mechanisms [59]. Thus, PunA's anticancer activity is unlikely to be explained by PPAR-γ signaling alone. Instead, our collective data suggests that PunA acts through a combination of mechanisms, modulating PPAR-γ while simultaneously promoting the lipid peroxidation that drives ferroptosis. Considering these activities are observed in OC cells but not normal cells, the proposed integrated metabolic and oxidative model would account for PunA's selective toxicity. Further studies are needed to define how PPAR-γ and PunA can be jointly leveraged in OC treatment.

Building on these observations of differential metabolic signaling, we next examined whether PunA also alters FAO, another key pathway linked to lipid metabolism and cancer cell survival [38]. We assessed expression of HADHA, a gene that encodes a core component of the mitochondrial trifunctional protein complex that regulates the rate of FAO activity [39]. PunA treatment increased HADHA expression in A2780 and HEYA8 cells but not in P201 or E7 cells, indicating enhanced FAO activity in OC cells relative to normal cells. (Figure 6B and 6C). Because mitochondrial FAO plays an important role in supplying energy to support proliferation, survival, drug resistance, and metastatic progression in cancer cells [38], this divergent response makes sense. Such reprogramming of OC cells to utilize FAO more heavily than normal cells may reflect an adaptive stress response that ultimately sensitize them to ferroptosis, consistent with our earlier findings on lipid peroxidation and PPAR-γ modulation.

Because FAO occurs in mitochondria, we next examined whether PunA also affects broader mitochondrial function. Seahorse XF analysis revealed that PunA significantly impaired mitochondrial respiration in HEYA8 cells by reducing basal and maximal respiration, ATP production, and spare respiratory capacity (Figure 7). This signals that PunA disrupts oxidative phosphorylation in OC cells, limiting their ability to meet energy demands and potentially amplifying oxidative stress that drives ferroptosis. Conversely, P201 cells exhibited minimal changes in mitochondrial function under the same conditions, mirroring their resistance to PunA-induced lipid peroxidation and ferroptosis. This selective preservation of mitochondrial activity suggests that normal cells maintain redox balance and mitochondrial integrity despite PunA exposure. These findings position mitochondria as a central mediator of PunA's selective toxicity. By impairing

 doi:10.20944/preprints202602.0821.v1

respiration and enhancing FAO-linked oxidative stress in OC cells, PunA exploits metabolic vulnerabilities that converge on ferroptotic cell death.

Finally, to explore the molecular basis of PunA's selective activity, we performed RNA-seq. PCA revealed clear separation between OC (HEYA8, A2780) and normal epithelial cells (P201, E7), as well as between PunA-treated and control groups (Figure 8A). This data indicates distinct transcriptional programs across cell types and treatment conditions. DEG analysis prior to PunA treatment showed that OC cells exhibited extensive dysregulation of genes involved in ECM remodeling, immune signaling, and tumor progression compared to normal cells (Figure 8B and C), consistent with known features of cancer biology. DEG analysis after PunA treatment revealed OC cells exhibited more long non-coding RNAs, pseudogenes, and unannotated transcripts compared to normal cells (Figure 8D and 8E). KEGG pathway analysis identified major differences in cytokine signaling, PI3K/Akt signaling, ECM organization, leukocyte migration, regulation of actin cytoskeleton, and calcium signaling pathway, human papillomavirus infection, and cell adhesion (Figure 8F).

We next focused on PunA-specific transcriptional responses. Consistent with PunA's stronger biological activity in OC cells, HEYA8 showed a substantially stronger transcriptional shift upon treatment than P201 (Figure 9A). PCA of these two lines further confirmed clear segregation between the treated and untreated groups (Figure 9B). KEGG enrichment showed that PunA-modulated genes were concentrated in pathways linked to lipid metabolism, inflammation, immune regulation, infection, and tumor progression (Figure 9C-E).

Importantly, our data suggest that PunA modulates the PI3K–Akt/mTOR pathway, a central regulator of OC proliferation and survival, which is consistent with prior evidence showing that metabolic stress and lipid derived signals can influence this axis [60,61]. We also observed PunA-dependent changes in cytokine–cytokine receptor signaling. Aberrant cytokine expression, particularly among CXCL, CCL, and IL family members, closely associated with immune cell infiltration, tumor immune microenvironment characteristics, and clinical prognosis [62–64]. In addition, PunA affected genes involved in cytoskeletal organization and calcium signaling. These pathways contribute to OC cell motility and the epithelial–mesenchymal transition (EMT), as previous work shows that calcium-dependent regulators like *TRPM7* can drive EMT through PI3K/Akt activation. Thus, beyond inhibiting proliferation, PunA may also impair migratory or invasive behavior by disrupting cytoskeletal or calcium signaling homeostasis. Together, these findings indicate that PunA reprograms multiple cancer-relevant signaling networks while exerting far weaker effects in normal cells. This selective network rewiring likely contributes to the anticancer activity of PunA and points toward a capacity to modulate tumor-immune interactions in OC.

In summary, our findings identify PunA as a promising selective anticancer agent, which we theorize to be driven largely by its ability to induce ferroptosis in OC cells while sparing normal cells. Across multiple experimental platforms, PunA consistently targeted cancer-specific vulnerabilities: it induced lipid peroxidation, upregulated PPAR-γ, disrupted mitochondrial respiration, enhanced FAO-dependent oxidative stress, and reprogrammed transcriptional networks associated with inflammation, immune regulation, and tumor progression. Pertinently, these effects were minimal in normal epithelial cells. Preliminary in vivo experiments, though limited in sample size, further suggested that PunA reduces tumor burden in immunocompetent mouse models. These data, taken together, highlight PunA's therapeutic potential and support its use alongside existing chemotherapy. Cisplatin remains a cornerstone of OC treatment but is restricted by dose-limiting toxicities such as nephrotoxicity and neurotoxicity [51]. Our results suggest that combining PunA with cisplatin-based chemotherapy may allow for dose reduction without loss of efficacy, thereby improving tolerability in clinical settings.

The major limitation of this study is the lack of sufficient animal studies, which will be essential to validate PunA's efficacy, safety, and pharmacokinetics in vivo. Nonetheless, PunA's nature as an omega-5 fatty acid and its strong cancer-specific effects suggest a favorable safety profile. Our preliminary animal data indicates that intraperitoneal delivery of PunA is feasible and well tolerated, offering a potentially effective route for delivery. Moving forward, comprehensive in vivo studies

 doi:10.20944/preprints202602.0821.v1

and eventual clinical trials will be critical to determine PunA's therapeutic value, both as a standalone agent and as and adjuvant to platinum-based chemotherapy for the treatment of OC.

Supplementary Materials: The following supporting information can be downloaded at: https://www.mdpi.com/article/doi/s1, Table S1: Gene Readcounts of All Samples; Table S2: Output GO All Result. Table S3: Output KEGG Result; Table S4: DEG HEYA8 vs P201 PunA Interaction; Table S5: Output GO All Result; Table S6: Output KEGG Result.

Author Contributions: Conceptualization, Z.H. and J.F.; methodology, Z.H.; software, J.M.; formal analysis, J.M., I.M., A.J.A., K.W., H.L., S.G., R.K., V.G., and Z.H.; investigation, J.M., I.M., A.J.A., K.W., H.L., S.G., V.G., R.K., E.N., and A.L.; writing—original draft preparation, J.M., I.M., A.J.A., K.W., H.L., S.G., V.G., and R.K.; writing—review and editing, I.M., J.F., and Z.H.; visualization, J.M., I.M., A.J.A., K.W., H.L., V.G., R.K., and S.G.; supervision, Z.H.; project administration, Z.H. and I.M.; funding acquisition, Z.H. All authors have read and agreed to the published version of the manuscript. J.M. and I.M. contributed equally to this paper. .

Funding: This project was supported by the NIH/NIA award R03 AG068685-01A1 NIH/NIA (PI: Zhiqing Huang), American Cancer Society-Duke Cancer Institute (ACS-DCI) Grant - Pilot Awards Spring 2024 (PI: Zhiqing Huang), and The Charles Hammond Research Fund (CHRF), Department of Obstetrics and Gynecology, Duke University School of Medicine (PI: Zhiqing Huang).

Institutional Review Board Statement. The animal study protocol was approved by Institutional Animal Care and Use Committee (IACUC) of DUKE UNIVERSITY (protocol code A223-21-11).

Data Availability Statement: Data availability statement: RNA-seq data are shown in Table S1-S6. All other raw data generated in this study are available upon request from the corresponding author. .

Acknowledgments: We thank Carole Grenier for providing technical training and laboratory support.

Conflicts of Interest: The authors declare that they have no known competing financial interests or personal relationships that could have influenced the work reported in this study.

Abbreviations

The following abbreviations are used in this manuscript:

OC	Ovarian cancer
FFA	Free fatty acid
PunA	Punicic acid
α-ESA	α-Eleostearic acid
TME	Tumor microenvironment
ECM	Extracellular matrix
AT	Adipose tissue
AME	Adipose tumor microenvironment
CAAs	Cancer-associated adipocytes
NFT	Normal fallopian tube
PPAR-γ	Peroxisome proliferator-activated receptor gamma
IP	Intraperitoneal
HGSOC	High grade serous ovarian cancer
DF	Differentiated
UD	Undifferentiated
Fer-1	Ferrostatin-1
FAO	Fatty acid oxidation
HADHA	Hydroxyacyl-CoA dehydrogenase trifunctional multienzyme subunit alpha
PCA	Principle component analysis
DEGs	Differentially expressed genes
lncRNA	Long non-coding RNA
GO	Gene ontology
MHC	Major histocompatibility complex

 doi:10.20944/preprints202602.0821.v1

ACSL4 Acyl-CoA synthetase long-chain family member 4
EMT Epithelial-mesenchymal transition

References

1. Ovarian cancer. https://www.mayoclinic.org/diseases-conditions/ovarian-cancer/symptoms-causes/syc-20375941
2. Key Statistics for Ovarian Cancer. Accessed 19. https://www.cancer.org/cancer/types/ovarian-cancer/key-statistics.html#ovarian-cancer-estimates-for-2025
3. Ali AT, Al-Ani O, Al-Ani F. Epidemiology and risk factors for ovarian cancer. Prz Menopauzalny. Jun 2023;22(2):93–104. doi:10.5114/pm.2023.128661
4. Loughran EA, Leonard AK, Hilliard TS, et al. Aging Increases Susceptibility to Ovarian Cancer Metastasis in Murine Allograft Models and Alters Immune Composition of Peritoneal Adipose Tissue. Neoplasia. Jun 2018;20(6):621–631. doi:10.1016/j.neo.2018.03.007
5. Mottini C, Auciello FR, Manni I, et al. The cross-talk between the macro and micro-environment in precursor lesions of pancreatic cancer leads to new and promising circulating biomarkers. J Exp Clin Cancer Res. Jul 18 2024;43(1):198. doi:10.1186/s13046-024-03117-5
6. Harper EI, Sheedy EF, Stack MS. With Great Age Comes Great Metastatic Ability: Ovarian Cancer and the Appeal of the Aging Peritoneal Microenvironment. Cancers (Basel). Jul 10 2018;10(7)doi:10.3390/cancers10070230
7. Lengyel E, Makowski L, DiGiovanni J, Kolonin MG. Cancer as a Matter of Fat: The Crosstalk between Adipose Tissue and Tumors. Trends Cancer. May 2018;4(5):374–384. doi:10.1016/j.trecan.2018.03.004
8. Duarte Mendes A, Freitas AR, Vicente R, et al. Adipocyte Microenvironment in Ovarian Cancer: A Critical Contributor? Int J Mol Sci. Nov 22 2023;24(23)doi:10.3390/ijms242316589
9. Jiang Y, Wang C, Zhou S. Targeting tumor microenvironment in ovarian cancer: Premise and promise. Biochim Biophys Acta Rev Cancer. Apr 2020;1873(2):188361. doi:10.1016/j.bbcan.2020.188361
10. Cai Q, Yang J, Shen H, Xu W. Cancer-associated adipocytes in the ovarian cancer microenvironment. Am J Cancer Res. 2024;14(7):3259–3279. doi:10.62347/XZRI9189
11. Wu Q, Li B, Sun S, Sun S. Unraveling Adipocytes and Cancer Links: Is There a Role for Senescence? Front Cell Dev Biol. 2020;8:282. doi:10.3389/fcell.2020.00282
12. Schaum N, Lehallier B, Hahn O, et al. Ageing hallmarks exhibit organ-specific temporal signatures. Nature. Jul 2020;583(7817):596–602. doi:10.1038/s41586-020-2499-y
13. Feng J, Rouse CD, Taylor L, et al. Regulation of Age-Related Lipid Metabolism in Ovarian Cancer. International Journal of Molecular Sciences. 2025;26(1):320. doi:10.3390/ijms26010320
14. Dhar Dubey KK, Sharma G, Kumar A. Conjugated Linolenic Acids: Implication in Cancer. J Agric Food Chem. Jun 5 2019;67(22):6091–6101. doi:10.1021/acs.jafc.9b01379
15. Yuan G-f, Chen X-E, Li D. Conjugated Linolenic Acids and Their Bioactivities: A Review. Food & Function. 2014 2014;5(7):1360–1368. doi:10.1039/c4fo00037d
16. Nugteren DH, Christ-Hazelhof E. Naturally occurring conjugated octadecatrienoic acids are strong inhibitors of prostaglandin biosynthesis. Prostaglandins. Mar 1987;33(3):403–17. doi:10.1016/0090-6980(87)90022-0
17. Gasmi J, Sanderson JT. Growth inhibitory, antiandrogenic, and pro-apoptotic effects of punicic acid in LNCaP human prostate cancer cells. J Agric Food Chem. Dec 8 2010;58(23):12149–56. doi:10.1021/jf103306k
18. Grossmann ME, Mizuno NK, Schuster T, Cleary MP. Punicic acid is an omega-5 fatty acid capable of inhibiting breast cancer proliferation. Int J Oncol. Feb 2010;36(2):421–6.
19. Quitmeyer B, Emelife C, Klausner H, Gbayisomore O, Phelan S. Differential Effects of Punicic Acid on Cytotoxicity and Peroxiredoxin Expression in MCF-7 Breast Cancer and MCF-10A Normal Cells. Anticancer Res. Nov 2024;44(11):4751–4759. doi:10.21873/anticanres.17301
20. Igarashi M, Miyazawa T. Newly recognized cytotoxic effect of conjugated trienoic fatty acids on cultured human tumor cells. Cancer Lett. Feb 1 2000;148(2):173–9. doi:10.1016/s0304-3835(99)00332-8
21. Zhang T, Gao Y, Mao Y, et al. Growth inhibition and apoptotic effect of alpha-eleostearic acid on human breast cancer cells. J Nat Med. Jan 2012;66(1):77–84. doi:10.1007/s11418-011-0556-4

22. Liu H, Liu S-L. Pharmacological Effects of Natural Components Against Ovarian Cancer and Mechanisms. In: Schatten H, ed. Ovarian Cancer: Molecular & Diagnostic Imaging and Treatment Strategies. Springer International Publishing; 2021:55–73.
23. Chan DW, Yung MMH, Chan Y-S, et al. MAP30 protein from Momordica charantia is therapeutic and has synergic activity with cisplatin against ovarian cancer in vivo by altering metabolism and inducing ferroptosis. Pharmacological Research. 2020/11/01/ 2020;161:105157. doi:https://doi.org/10.1016/j.phrs.2020.105157
24. Pitchakarn P, Umsumarng S, Mapoung S, et al. Kuguacin J isolated from bitter melon leaves modulates paclitaxel sensitivity in drug-resistant human ovarian cancer cells. Journal of Natural Medicines. 2017/10/01 2017;71(4):693–702. doi:10.1007/s11418-017-1099-0
25. Yung MMH, Ross FA, Hardie DG, et al. Bitter Melon (Momordica charantia) Extract Inhibits Tumorigenicity and Overcomes Cisplatin-Resistance in Ovarian Cancer Cells Through Targeting AMPK Signaling Cascade. Integrative Cancer Therapies. 2016;15(3):376–389. doi:10.1177/1534735415611747
26. Song HK, Hwang DY. Use of C57BL/6N mice on the variety of immunological researches. Lab Anim Res. Jun 2017;33(2):119–123. doi:10.5625/lar.2017.33.2.119
27. Rose PG. First-Line Chemotherapy for Ovarian Cancer: Inferences From Recent Studies. Oncologist. Nov 2016;21(11):1286–1290. doi:10.1634/theoncologist.2016-0144
28. Prat J, D'Angelo E, Espinosa I. Ovarian carcinomas: at least five different diseases with distinct histological features and molecular genetics. Human Pathology. 2018/10/01/ 2018;80:11–27. doi:https://doi.org/10.1016/j.humpath.2018.06.018
29. Hobbs C, Huang Z, Murphy S, Berchuck A. The function of matrix metalloproteinase 1 in ovarian cancer. Gynecologic Oncology. 2019;154:80. doi:10.1016/j.ygyno.2019.04.189
30. Romani AMP. Cisplatin in cancer treatment. Biochemical Pharmacology. 2022/12/01/ 2022;206:115323. doi:10.1016/j.bcp.2022.115323
31. Abu Samaan TM, Samec M, Liskova A, Kubatka P, Büsselberg D. Paclitaxel's Mechanistic and Clinical Effects on Breast Cancer. Biomolecules. Nov 27 2019;9(12)doi:10.3390/biom9120789
32. Baumann KE, Siamakpour-Reihani S, Dottino J, et al. High-fat diet and obesity are associated with differential angiogenic gene expression in epithelial ovarian cancer. Gynecologic Oncology. 2023;179:97–105. doi:10.1016/j.ygyno.2023.11.002
33. Martina Strnadová DT, and Isabell Kaczmarek. Utilizing the property of differentiated 3T3-L1 cells to produce fats in the cell culture medium, we induced cell differentiation by insulin induction. Protocols. Star Protocols. June 6, 2024;doi:https://star-protocols.cell.com/protocols/3504
34. Kim JW, Lee J-Y, Oh M, Lee E-W. An integrated view of lipid metabolism in ferroptosis revisited via lipidomic analysis. Experimental & Molecular Medicine. 2023/08/01 2023;55(8):1620–1631. doi:10.1038/s12276-023-01077-y
35. Sun D, Wang L, Wu Y, et al. Lipid metabolism in ferroptosis: mechanistic insights and therapeutic potential. Front Immunol. 2025;16:1545339. doi:10.3389/fimmu.2025.1545339
36. Do Q, Xu L. How do different lipid peroxidation mechanisms contribute to ferroptosis? Cell Rep Phys Sci. Dec 20 2023;4(12)doi:10.1016/j.xcrp.2023.101683
37. Cheng HS, Yip YS, Lim EKY, Wahli W, Tan NS. PPARs and Tumor Microenvironment: The Emerging Roles of the Metabolic Master Regulators in Tumor Stromal-Epithelial Crosstalk and Carcinogenesis. Cancers (Basel). Apr 29 2021;13(9)doi:10.3390/cancers13092153
38. Ma J, Wang S, Zhang P, et al. Emerging roles for fatty acid oxidation in cancer. Genes & Diseases. 2025/07/01/ 2025;12(4):101491. doi:https://doi.org/10.1016/j.gendis.2024.101491
39. Wang X, Song H, Liang J, Jia Y, Zhang Y. Abnormal expression of HADH, an enzyme of fatty acid oxidation, affects tumor development and prognosis (Review). Mol Med Rep. Dec 2022;26(6)doi:10.3892/mmr.2022.12871
40. Peng Y, Zhang L, Zhang M. Comprehensive Analysis of Genomic Instability Derived lncRNAs Prognostic Signature and the Associated Tumor Microenvironment in Glioma. American Journal of Medical Genetics Part B: Neuropsychiatric Genetics. 2026;201(1):64–88. doi:https://doi.org/10.1002/ajmg.b.33044

 doi:10.20944/preprints202602.0821.v1

41. Zhang X, Li M, Sun G, Bai Y, Lv D, Liu C. MiR-563 restrains cell proliferation via targeting LIN28B in human lung cancer. Thoracic Cancer. 2020;11(1):55–61. doi:https://doi.org/10.1111/1759-7714.13257
42. Antonarakis SE. Small nuclear RNA genes in Mendelian disorders. Nature Genetics. 2025/12/04 2025;doi:10.1038/s41588-025-02440-7
43. Labidi-Galy SI, Papp E, Hallberg D, et al. High grade serous ovarian carcinomas originate in the fallopian tube. Nat Commun. Oct 23 2017;8(1):1093. doi:10.1038/s41467-017-00962-1
44. Lin A, Giuliano CJ, Palladino A, et al. Off-target toxicity is a common mechanism of action of cancer drugs undergoing clinical trials. Science Translational Medicine. 2019;11(509):eaaw8412. doi:doi:10.1126/scitranslmed.aaw8412
45. Ma LL, Liang L, Zhou D, Wang SW. Tumor suppressor miR-424-5p abrogates ferroptosis in ovarian cancer through targeting ACSL4. Neoplasma. Jan 2021;68(1):165–173. doi:10.4149/neo_2020_200707N705
46. Jiang X, Stockwell BR, Conrad M. Ferroptosis: mechanisms, biology and role in disease. Nature Reviews Molecular Cell Biology. 2021/04/01 2021;22(4):266–282. doi:10.1038/s41580-020-00324-8
47. Vermonden P, Martin M, Glowacka K, et al. Phospholipase PLA2G7 is complementary to GPX4 in mitigating punicic-acid-induced ferroptosis in prostate cancer cells. iScience. 2024;27(5)doi:10.1016/j.isci.2024.109774
48. Vermonden P, Vancoppenolle M, Dierge E, et al. Punicic Acid Triggers Ferroptotic Cell Death in Carcinoma Cells. Nutrients. Aug 10 2021;13(8)doi:10.3390/nu13082751
49. Dasari S, Bernard Tchounwou P. Cisplatin in cancer therapy: Molecular mechanisms of action. European Journal of Pharmacology. 2014/10/05/ 2014;740:364–378. doi:10.1016/j.ejphar.2014.07.025
50. Duarte D, Vale N. Evaluation of synergism in drug combinations and reference models for future orientations in oncology. Current Research in Pharmacology and Drug Discovery. 2022/01/01/ 2022;3:100110. doi:https://doi.org/10.1016/j.crphar.2022.100110
51. Alderden RA, Hall MD, Hambley TW. The Discovery and Development of Cisplatin. Journal of Chemical Education. 2006/05/01 2006;83(5):728. doi:10.1021/ed083p728
52. Chehade H, Tedja R, Ramos H, et al. Regulatory Role of the Adipose Microenvironment on Ovarian Cancer Progression. Cancers. 2022;14(9):2267.
53. Li Z, Fang X, Wang S. Omentum provides a special cell microenvironment for ovarian cancer. Cancer Rep (Hoboken). Oct 2023;6(10):e1858. doi:10.1002/cnr2.1858
54. Li J, Cao F, Yin H-l, et al. Ferroptosis: past, present and future. Cell Death & Disease. 2020/02/03 2020;11(2):88. doi:10.1038/s41419-020-2298-2
55. Janani C, Ranjitha Kumari BD. PPAR gamma gene – A review. Diabetes & Metabolic Syndrome: Clinical Research & Reviews. 2015/01/01/ 2015;9(1):46–50. doi:https://doi.org/10.1016/j.dsx.2014.09.015
56. Krishnan A, Nair SA, Pillai MR. Biology of PPAR gamma in cancer: a critical review on existing lacunae. Curr Mol Med. Sep 2007;7(6):532–40. doi:10.2174/156652407781695765
57. Yang L, Yuan J, Liu L, et al. α-linolenic acid inhibits human renal cell carcinoma cell proliferation through PPAR-γ activation and COX-2 inhibition. Oncol Lett. 2013/07/01 2013;6(1):197–202. doi:10.3892/ol.2013.1336
58. Gupta RA, Brockman JA, Sarraf P, Willson TM, DuBois RN. Target Genes of Peroxisome Proliferator-activated Receptor γ in Colorectal Cancer Cells *. Journal of Biological Chemistry. 2001;276(32):29681–29687. doi:10.1074/jbc.M103779200
59. Gou Q, Gong X, Jin J, Shi J, Hou Y. Peroxisome proliferator-activated receptors (PPARs) are potential drug targets for cancer therapy. Oncotarget. Sep 1 2017;8(36):60704–60709. doi:10.18632/oncotarget.19610
60. He Y, Sun MM, Zhang GG, et al. Targeting PI3K/Akt signal transduction for cancer therapy. Signal Transduct Target Ther. Dec 16 2021;6(1):425. doi:10.1038/s41392-021-00828-5
61. Janku F, Wheler JJ, Westin SN, et al. PI3K/AKT/mTOR inhibitors in patients with breast and gynecologic malignancies harboring PIK3CA mutations. J Clin Oncol. Mar 10 2012;30(8):777–82. doi:10.1200/jco.2011.36.1196
62. Fan L, Lei H, Lin Y, et al. Identification of a Gene Set Correlated With Immune Status in Ovarian Cancer by Transcriptome-Wide Data Mining. Front Mol Biosci. 2021;8:670666. doi:10.3389/fmolb.2021.670666
63. Zhang T, Ren Y, Yang P, Wang J, Zhou H. Cancer-associated fibroblasts in pancreatic ductal adenocarcinoma. Cell Death Dis. Oct 25 2022;13(10):897. doi:10.1038/s41419-022-05351-1

 doi:10.20944/preprints202602.0821.v1

64. Li J, Sun J, Zeng Z, et al. Tumour-associated macrophages in gastric cancer: From function and mechanism to application. Clin Transl Med. Aug 2023;13(8):e1386. doi:10.1002/ctm2.1386